Journal of Medicinal Chemistry

Article

pubs.acs.org/jmc

Discovery of 1-{4-[3-Fluoro-4-((3*S*,6*R*)-3-methyl-1,1-dioxo-6-phenyl-[1,2]thiazinan-2-ylmethyl)-phenyl]-piperazin-1-yl}-ethanone (GNE-3500): a Potent, Selective, and Orally Bioavailable Retinoic Acid Receptor-Related Orphan Receptor C (RORc or RORγ) Inverse Agonist

Benjamin P. Fauber,*[,†] Olivier René,[†] Yuzhong Deng,[‡] Jason DeVoss,[§] Céline Eidenschenk,[§] Christine Everett,[∥] Arunima Ganguli,[⊥] Alberto Gobbi,[†] Julie Hawkins,[⊥] Adam R. Johnson,[∥] Hank La,[‡] Justin Lesch,[§] Peter Lockey,[⊥] Maxine Norman,[⊥] Wenjun Ouyang,[§] Susan Summerhill,[⊥] and Harvey Wong[‡]

[†]Discovery Chemistry, [‡]Drug Metabolism and Pharmacokinetics, [§]Immunology, [∥]Biochemical Pharmacology, Genentech, Inc., 1 DNA Way, South San Francisco, California 94080, United States

[⊥]Discovery Biology, Argenta, Units 7-9 Spire Green Centre, Flex Meadow, Harlow, Essex CM19 5TR, U.K.

Supporting Information

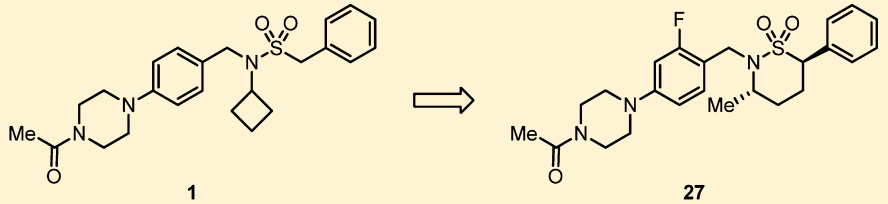

1
RORc human transcription cell EC_{50} = 130 nM
HLM CL_{hep} = 19 mL/min/kg
RLM CL_{hep} = 47 mL/min/kg

27
RORc human transcription cell EC_{50} = 47 nM
HLM CL_{hep} = 10 mL/min/kg
Rat CL_p = 12 mL/min/kg
Rat *F*% = 55%

ABSTRACT: Retinoic acid receptor-related orphan receptor C (RORc, RORγ, or NR1F3) is a nuclear receptor that plays a major role in the production of interleukin (IL)-17. Considerable efforts have been directed toward the discovery of selective RORc inverse agonists as potential treatments of inflammatory diseases such as psoriasis and rheumatoid arthritis. Using the previously reported tertiary sulfonamide **1** as a starting point, we engineered structural modifications that significantly improved human and rat metabolic stabilities while maintaining a potent and highly selective RORc inverse agonist profile. The most advanced δ-sultam compound, GNE-3500 (**27**, 1-{4-[3-fluoro-4-((3*S*,6*R*)-3-methyl-1,1-dioxo-6-phenyl-[1,2]thiazinan-2-ylmethyl)-phenyl]-piperazin-1-yl}-ethanone), possessed favorable RORc cellular potency with 75-fold selectivity for RORc over other ROR family members and >200-fold selectivity over 25 additional nuclear receptors in a cell assay panel. The favorable potency, selectivity, in vitro ADME properties, in vivo PK, and dose-dependent inhibition of IL-17 in a PK/PD model support the evaluation of **27** in preclinical studies.

INTRODUCTION

The nuclear receptor (NR) retinoic acid receptor-related orphan receptor C (RORc or RORγ, also known as NR1F3)[1] is an important transcription factor involved in the production and regulation of the pro-inflammatory cytokine interleukin (IL)-17.[2] Antibodies inhibiting the production or activity of IL-17 family cytokines[3,4] have demonstrated proof of concept in clinical trials for the treatment of psoriasis,[5−7] rheumatoid arthritis (RA),[8] ankylosing spondylitis,[9] and uveitis.[10] RORc also plays a role in the regulation of IL-22[11] and granulocyte macrophage colony stimulating factor (GM-CSF)[12] as well as the production of innate lymphoid cells (ILCs)[13,14] and γδ T cells.[15] On the basis of the influence of RORc over multiple inflammatory pathways, it has been proposed that RORc is a potentially valuable molecular target for the treatment of inflammatory diseases.[16−22]

Our group has previously reported the discovery and optimization of tertiary sulfonamide RORc inverse agonists,[23−26] as exemplified by **1** (Scheme 1). Compound **1** was a potent RORc inverse agonist in a biochemical assay (EC_{50} = 30 nM), GAL4 human transcription cell assay (EC_{50} = 130 nM), and human peripheral blood mononuclear cell (PBMC) assay (EC_{50} = 800 nM).[25] Compound **1** was also >77-fold selective for RORc over other NRs as assessed by a panel of GAL4 human transcription cell assays.[25] When **1** was incubated with human or rat liver microsomes (HLM or RLM), however, it displayed high hepatic clearance (CL_{hep}) values in both species (>70% of liver blood flow),[25] thereby limiting its utility to in vitro experiments.

Received: April 17, 2015

DOI: 10.1021/acs.jmedchem.5b00597
J. Med. Chem. XXXX, XXX, XXX−XXX

Scheme 1. Identification of the Human and Rodent in Vitro Metabolites of 1[a]

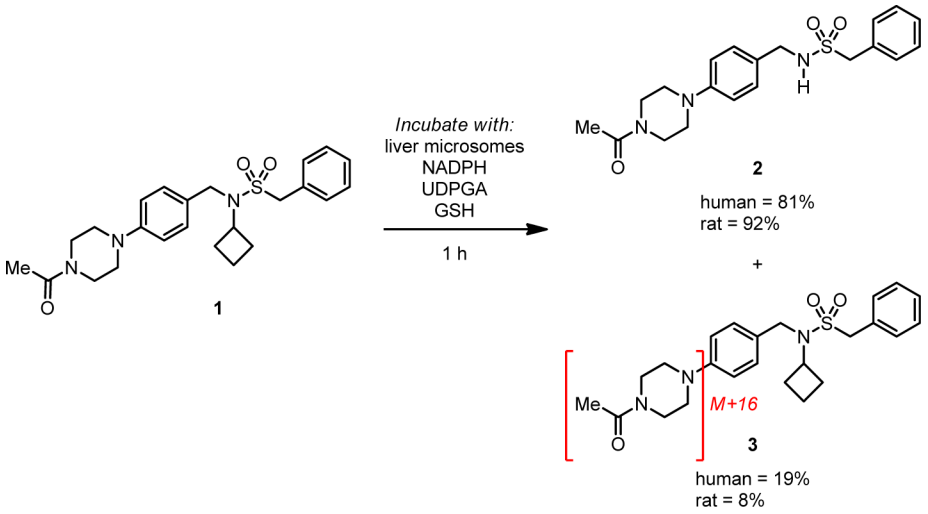

[a]Compound **1** was completely metabolized in both human and rat liver microsomes over the course of the 1 h in vitro studies. Metabolites are shown as a percentage of all detected compounds (LC-MS/MS method) at the end of the studies. The studies were conducted using nonisotopic **1**.

Metabolite identification (MetID) studies with either HLM or RLM revealed that **1** (Scheme 1) was completely consumed during the 1 h incubation period and two metabolites were formed. The major metabolite in both the HLM and RLM studies was the sulfonamide *N*-dealkylation product **2** (human = 81%, rat = 92%), and oxidation of the piperazine ring (M + 16) provided the minor metabolite **3** (human = 19%, rat = 8%). Metabolite **2** was inactive in the RORc SRC1 biochemical assay (EC_{50} > 10 μM). On the basis of the MetID data, we devised a strategy to address the *N*-dealkylation metabolism and improve the metabolic stability of compounds related to **1** while also maintaining favorable RORc inverse agonist potency.

RESULTS AND DISCUSSION

The synthesis of **1** was described in our lab's previous article.[25] Compound **6** (Scheme 2) was synthesized through the sulfonylation of 2-amino-2-methylpropanenitrile (**4**) with phenylmethanesulfonyl chloride to provide the secondary sulfonamide intermediate (**5**). Benzylation of the secondary sulfonamide under basic conditions using 1-bromo-4-(bromomethyl)benzene, followed by Buchwald–Hartwig amination[27] of the aryl-bromide with *N*-acetylpiperazine, led to an in situ cyclization reaction[28] to form **6**. Compound **6** was the only product of the reaction.

Scheme 2. Synthesis of 6[a]

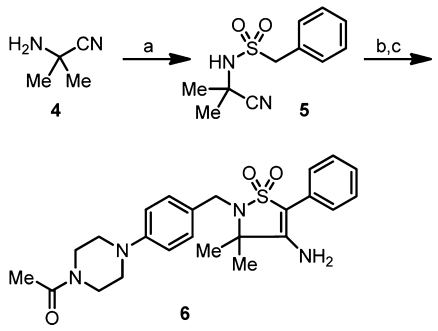

[a]Reagents and conditions: (a) $BnSO_2Cl$, $EtN(i\text{-}Pr)_2$, DCM, 23 °C, 46%; (b) 1-bromo-4-(bromomethyl)benzene, NaH, DMA, 75 °C; (c) *N*-acetylpiperazine, RuPhos Pd G1 MTBE adduct, RuPhos, NaO*t*-Bu, 1,4-dioxane, 100 °C, 14% over 2 steps.

Syntheses of the sultam analogues originated from the corresponding amino-halides (**7**–**8**, Scheme 3) or amino-alcohols (**9**–**11**),[29] and the sultam rings were assembled according to the method of Lee et al.[30] Compounds **7**–**8** were reacted with phenylmethanesulfonyl chloride and triethylamine to yield the secondary sulfonamides, followed by treatment with two equivalents of base to facilitate cyclization to the sultam ring intermediates (**12**–**13**). In an analogous manner to **7**–**8**, compounds **9**–**11** were reacted with two equivalents of phenylmethanesulfonyl chloride and triethylamine, followed by treatment of the crude reaction products with NaCl in hot DMF to form the alkyl chloride intermediates. The crude alkyl chloride intermediates were reacted with two equivalents of base to form the sultam ring intermediates (**14**–**16**). Compounds **12**–**16** were exposed to sodium hydride and 4-bromo-1-(bromomethyl)-2-fluorobenzene to provide the crude *N*-benzyl sultam intermediates. The *N*-benzyl intermediates were then carried forward into a Buchwald–Hartwig amination[27] with *N*-acetylpiperazine to provide the sultam products as mixtures of enantiomers and diastereomers (**17**–**21**). The stereoisomers of the δ-sultam products were separated by chiral supercritical fluid chromatography (SFC) to provide the enantiopure products (**22**–**29**). The absolute stereochemistry of the (6*R*)-phenyl δ-sultam ring in **23** was assigned by single-crystal X-ray analysis (see Supporting Information). The absolute stereochemistry of the 6-phenyl substituent on the (3*R*)- and (3*S*)-methyl δ-sultam products (**24**–**27**) were assigned by NMR analysis.[31] We obtained a single-crystal X-ray structure of **27** to further confirm the absolute stereochemistry of the (6*R*)-phenyl δ-sultam ring (see Supporting Information). The X-ray data for **27** was in agreement with the stereochemistry we had originally assigned by NMR.[31] Repeated attempts to crystallize either **28** or **29** for X-ray analysis were unsuccessful. Thus, the stereochemistry of the 6-phenyl substituent in **28** and **29** was assigned based on their relative optical rotations to **22** and **23**, respectively (i.e., optical

DOI: 10.1021/acs.jmedchem.5b00597
J. Med. Chem. XXXX, XXX, XXX–XXX

Scheme 3. Syntheses of Sultam Analogues[a]

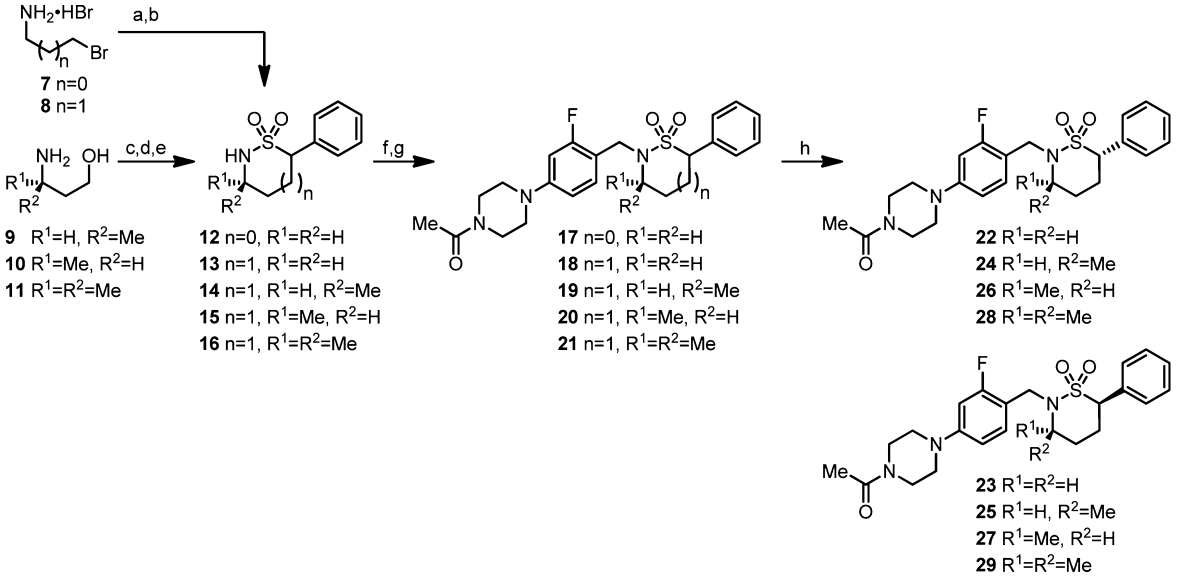

[a]Reagents and conditions: (a) $BnSO_2Cl$, Et_3N, THF, 0 → 23 °C; (b) *n*-BuLi, $(i\text{-Pr})_2NH$, phenanthroline, THF, −78 °C, 42−59% over 2 steps; (c) $BnSO_2Cl$, Et_3N, THF, 0 → 23 °C; (d) NaCl, DMF, 80 °C; (e) *n*-BuLi, $(i\text{-Pr})_2NH$, phenanthroline, THF, −78 °C, 21−42% over 3 steps; (f) 4-bromo-1-(bromomethyl)-2-fluorobenzene, NaH, DMF, 0 °C; (g) $Pd(OAc)_2$, RuPhos, Cs_2CO_3, *N*-acetylpiperazine, 1,4-dioxane, 80 °C, 16−73% over 2 steps; (h) chiral column SFC purification.

Table 1. Structure−Activity Relationships and in Vitro Metabolism

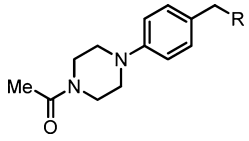

compd	R-group	RORc SRC1 EC_{50}[a] (μM) [%eff]	cLogP[b]	LLE[c]	HLM CL_{hep}[d] (mL/min/kg)	RLM CL_{hep}[e] (mL/min/kg)
1	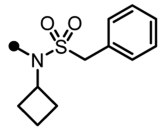	0.031 [-99%]	3.2	4.3	19	47
30	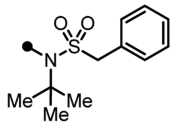	0.031 [-99%]	3.4	3.8	20	47
6	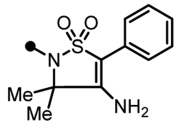	>10 [-10%]	3.6	-	5	8

[a]Inhibition of human RORc-LBD recruitment of the SRC1 coactivator peptide where the EC_{50} values are reported as means (all standard deviations were <55% of the mean EC_{50} values) for ≥3 separate titrations; percent efficacy "%eff" is the maximal efficacy observed in the assay at the highest test concentration of 10 μM, and the %eff values are reported as means (all standard deviations were <4% of the mean %eff values); negative %eff denotes inverse agonism of the basal activity of apo-RORc-LBD in this assay format. [b]Calculated Log *P* (cLogP) value.[55] [c]Ligand-lipophilicity efficiency (LLE) was calculated using the equation: LLE = (RORc SRC1 pEC_{50}) − cLogP.[34,35] [d]Predicted human clearance extrapolated from in vitro human liver microsome (HLM) experiments. [e]Predicted rat clearance extrapolated from in vitro rat liver microsome (RLM) experiments.

comparison),[32] in addition to their biochemical potencies and metabolic stabilities in relation to stereoisomers **22**−**27**. The syntheses of compounds **30**[25] (Table 1) and **31**[23] (Table 2) were described in our lab's previous manuscripts.

The analogues were tested in a time-resolved fluorescence biochemical assay that monitored the ability of the human RORc ligand binding domain (LBD) to bind to a coactivator peptide derived from steroid receptor coactivator (SRC)-1.[33] Compounds that disrupted the recruitment of the SRC1 coactivator peptide and decreased the basal level of RORc signaling were inverse agonists. We also monitored the ligand-lipophilicity efficiency (LLE)[34,35] of the analogues with a goal of maintaining an LLE value comparable to or superior to that of **1** (LLE = 4.3). Tracking the LLE values ensured that we

DOI: 10.1021/acs.jmedchem.5b00597
J. Med. Chem. XXXX, XXX, XXX−XXX

Table 2. Structure–Activity Relationships and in Vitro Metabolism of Sultams

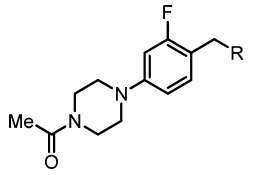

compd	R-group	RORc SRC1 EC_{50}[a] (μM) [%eff]	cLogP[b]	LLE[c]	HLM CL_{hep}[d] (mL/min/kg)	RLM CL_{hep}[e] (mL/min/kg)
31	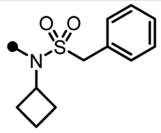	0.011 [-99%]	3.3	4.7	19	50
17	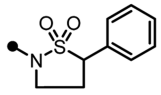	>10 [-22%]	3.0	-	13	31
18	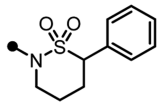	0.35 [-100%]	3.4	3.1	13	29
22	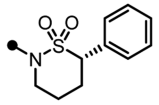	1.2 [-85%]	3.4	2.5	18	47
23	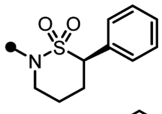	0.18 [-98%]	3.4	3.3	9	16
24	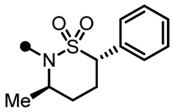	5.4 [-61%]	3.8	1.5	18	47
25	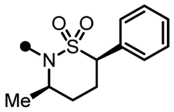	0.017 [-99%]	3.8	4.0	13	27
26	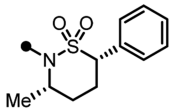	0.096 [-98%]	3.8	3.2	18	44
27	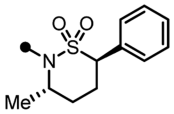	0.012 [-98%]	3.8	4.2	10	21
28	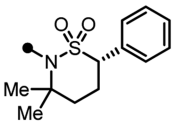	>10 [-45%]	4.5	-	18	35
29	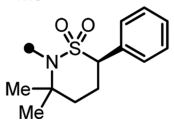	0.082 [-99%]	4.5	2.6	13	33

[a]Inhibition of human RORc-LBD recruitment of the SRC1 coactivator peptide where the EC_{50} values are reported as means (all standard deviations were <36% of the mean EC_{50} values) for ≥3 separate titrations; percent efficacy "%eff" is the maximal efficacy observed in the assay at the highest test concentration of 10 μM, and the %eff values are reported as means (all standard deviations were <5% of the mean %eff values); negative %eff denotes inverse agonism of the basal activity of apo-RORc-LBD in this assay format. [b]Calculated Log *P* (cLogP) value.[55] [c]Ligand-lipophilicity efficiency (LLE) was calculated using the equation: LLE = (RORc SRC1 pEC_{50}) − cLogP.[34,35] [d]Predicted human hepatic clearance extrapolated from in vitro human liver microsome (HLM) experiments. [e]Predicted rat hepatic clearance extrapolated from in vitro rat liver microsome (RLM) experiments.

were maintaining efficient binding interactions with the human RORc-LBD as we evolved the analogues and avoided the inclusion of unnecessary lipophilicity.

Other teams have successfully addressed the metabolic cleavage of *N*-alkyl groups on tertiary sulfonamides by lowering the lipophilicity of the *N*-alkyl substituent.[36] Unfortunately, this

DOI: 10.1021/acs.jmedchem.5b00597
J. Med. Chem. XXXX, XXX, XXX–XXX

approach was not tolerated in our tertiary sulfonamide series and led to compounds devoid of detectable RORc inverse agonist biochemical activity with no notable improvements in microsomal stability. We hypothesized that the major metabolite of **1** (Scheme 1) arose from oxidation of the *N*-alkyl group to generate an unstable aminal intermediate, followed by cleavage of the C−N bond to form **2**. Replacement of the hydrogen atoms on the *N*-alkyl carbon atom adjacent to the nitrogen with methyl groups should block this process. Indeed, when we synthesized the *N*-*tert*-butyl sulfonamide analogue (**30**, Table 1), this structural change abated the microsome-mediated cleavage of the *N*-*tert*-butyl group. Instead, we observed a new metabolite in which cleavage of the *N*-benzylic group of **30** was the major metabolite in MetID studies, and **30** provided no improvement in HLM and RLM CL_{hep} values as compared to **1**.

In addition to **30**, we explored other metabolically stable *tert*-butyl isosteres.[37] During the attempted synthesis of a *N*-(2-methylpropanenitrile)sulfonamide analogue, we observed the formation of a 4-amino-2,3-dihydroisothizaole 1,1-dioxide product (**6**, Table 1). Although **6** had no detectable RORc inverse agonist activity in our biochemical assay (EC_{50} > 10 μM), it possessed favorable HLM and RLM values (CL_{hep} = 5 and 8 mL/min/kg, respectively). This result led us to evaluate other cyclic sulfonamide (sultam) analogues as potential metabolically stable and potent RORc inverse agonists.

We utilized a fluorinated benzylic core in subsequent analogues that built on the promising results of **6**, as we have previously shown that inclusion of the fluorine atom provided improvements in RORc biochemical and cellular potencies.[23] We were aware of the lipophilic environment in the RORc ligand binding pocket surrounding the benzylic sulfonamide moiety of **31** (Table 2 and Figure 1) based on our previous RORc structure-based drug design campaigns.[23,25] We envisioned that removal of the somewhat polar 4-amino group found in the 2,3-dihydroisothizaole 1,1-dioxide ring of **6** could potentially improve the RORc affinity of closely related analogues. A 5-phenyl γ-sultam (**17**) provided a simplified scaffold in which to test this hypothesis. Compound **17** maintained moderate clearance values in the HLM and RLM assays (CL_{hep} = 13 and 31 mL/min/kg, respectively), but **17** had no RORc inverse agonist activity up to a 10 μM concentration in our biochemical assay. Encouraged by the favorable CL_{hep} values for **17** in comparison to **31**, we synthesized the 6-phenyl δ-sultam analogue (**18**). Compound **18** displayed moderate clearance values in the HLM and RLM assays (CL_{hep} = 13 and 29 mL/min/kg, respectively) and was also a RORc inverse agonist in our biochemical assay (EC_{50} = 350 nM). Separation of **18** into its two respective enantiomers provided **22** and **23**. Compound **22** displayed high clearance values in the HLM and RLM assays (CL_{hep} = 18 and 47 mL/min/kg, respectively), whereas **23** displayed moderate clearance values in the HLM and RLM assays (CL_{hep} = 9 and 16 mL/min/kg, respectively). Compound **23** was also 7-fold more potent than **22** in the RORc SRC1 biochemical assay (EC_{50} = 180 nM and 1.2 μM, respectively). To our delight, the more potent 6-phenyl δ-sultam enantiomer was also the more metabolically stable enantiomer. We hypothesized that the improved metabolic stability of **23** over **22** was potentially due to a steric clash of the (6*R*)-phenyl δ-sultam in **23** with the cytochrome P450 (CYP) that was responsible for the increased metabolic turnover of **22**.

On the basis of the encouraging metabolic stability and potency of **23**, we envisioned a refined strategy to accurately define the stereochemistry of the (6*R*)-phenyl group of the δ-sultam ring in future analogues while also improving the RORc inverse agonist potency of **23**. Introduction of a 3-methyl group with known absolute stereochemistry on the δ-sultam ring allowed such an opportunity.[31] Molecular modeling of the binding mode of **23** (Figure 1)[38] suggested that the 3-position of the δ-sultam ring provided access to a region of the ligand binding pocked filled by the *N*-alkyl substituent of **31** and other previously disclosed anlogues.[23,25]

The assay results for the (3*R*)-methyl-6-phenyl δ-sultam analogues **24** and **25** (Table 2) confirmed the initial observations made with **22** and **23**. Compound **24** had poor HLM and RLM stabilities (CL_{hep} = 18 and 47 mL/min/kg, respectively) and modest RORc inverse agonist biochemical potency (EC_{50} = 5.4 μM). Compound **25** had moderate HLM and RLM stabilities (CL_{hep} = 13 and 27 mL/min/kg, respectively) and was a potent RORc inverse agonist in the SRC1 biochemical assay (EC_{50} = 17 nM). The trend of the (6*R*)-phenyl group being the preferred δ-sultam stereoisomer was further supported with the assay results of the (3*S*)-methyl-6-phenyl δ-sultam analogues **26** and **27**. Although **26** had an improved RORc inverse agonist potency (EC_{50} = 94 nM) as compared with **24**, its 3-methyl stereochemical matched molecular pair,[39] **26** had poor HLM and RLM stabilities (CL_{hep} = 18 and 44 mL/min/kg, respectively). The (3*S*)-methyl-(6*R*)-phenyl δ-sultam analogue **27** (GNE-3500, 1-{4-[3-fluoro-4-((3*S*,6*R*)-3-methyl-1,1-dioxo-6-phenyl-[1,2]thiazinan-2-ylmethyl)-phenyl]-piperazin-1-yl}-ethanone) provided a very favorable overall profile with moderate HLM and RLM stabilities (CL_{hep} = 10 and 21 mL/min/kg, respectively) and potent RORc inverse agonist biochemical activity (EC_{50} = 12 nM). Compound **27** also displayed a favorable LLE value (LLE = 4.2) that was comparable to **1**.

The 3,3-dimethyl-6-phenyl δ-sultam enantiomers were tested to further probe the role of the 3-substituent in improving the RORc biochemical potency. The trend of one 6-phenyl δ-sultam isomer being more potent and metabolically stable

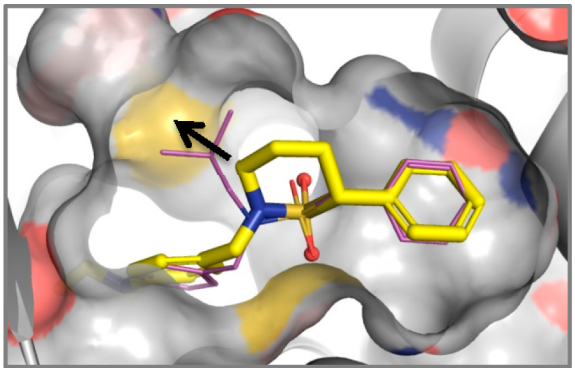

Figure 1. X-ray costructure of the human RORc-LBD (gray) and a tertiary sulfonamide RORc inverse agonist ligand (magenta lines) (PDB: 4WQP) modeled with **23** (yellow sticks).[38] The surface of the RORc-LBD ligand binding pocket is shown as an opaque surface (red and blue = polar residues, gray and yellow = lipophilic residues) and culled to reveal the bound (magenta lines) and modeled (yellow sticks) ligands. The arrow (black) illustrates a potential vector from the 3-position of the δ-sultam ring to fill the same region occupied by the *i*-butyl group of the RORc inverse agonist ligand (magenta lines) in the RORc-LBD X-ray costructure.

DOI: 10.1021/acs.jmedchem.5b00597
J. Med. Chem. XXXX, XXX, XXX−XXX

Table 3. In Vitro ADME Properties[a]

compd	human PPB (%bound)	rat PPB (%bound)	MDCK P_{app}[b] A→B (10^{-6} cm/s)	MDCK P_{app}[b] B→A (10^{-6} cm/s)	solubility[c] (μM)
31	98	98	22	24	21
23	94	95	27	29	22
25	95	96	16	19	43
26	96	96	23	16	34
27	95	95	24	32	20
29	98	96	17	11	34

[a]See the Supporting information for experimental details associated with each assessment. [b]Madin−Darby canine kidney (MDCK) cell permeability assay to assess membrane permeability (P_{app}); A→B, apical-to-basolateral; B→A, basolateral-to-apical.[41] [c]Aqueous kinetic solubility at pH 7.4 (measured in a high-throughput assay).

than the other also held true with these analogues. Compound **28** (Table 2) was less potent (RORc SRC1 EC_{50} > 10 μM) and less metabolically stable (HLM and RLM CL_{hep} = 18, 35 mL/min/kg, respectively) than **29** (RORc SRC1 EC_{50} = 82 nM; HLM and RLM CL_{hep} = 13, 33 mL/min/kg, respectively).

Compounds **23**, **25**, **26**, **27**, **29**, and **31** were evaluated in a suite of in vitro ADME assays[40] to assess their human and rat plasma-protein binding (PPB), Madin−Darby canine kidney (MDCK) cellular permeability,[41] and aqueous kinetic solubility at pH 7.4 (Table 3). We were encouraged to see that the favorable in vitro ADME profiles of the tertiary sulfonamide compounds exemplified by **31** (Table 3) were maintained in the δ-sultam subseries. The (6*R*)-phenyl δ-sultam analogues **23**, **25**, **27**, and **29** all possessed reasonable human and rat PPB values (%bound = 95−98% across both species) while also maintaining high apparent permeability ($P_{app(A\to B)}$ = 16−27 × 10^{-6} cm/s) with minimal efflux ($0.5 < (P_{app(A\to B)}/P_{app(B\to A)}) < 2$) in the MDCK assay. The kinetic aqueous solubility values of **23**, **25**, **27**, and **29** at pH 7.4 (20−43 μM) were also comparable to **31** (21 μM). Compound **26**, the stereochemical molecular matched pair of **27**, also possessed reasonable human and rat PPB values (%bound = 96% in both species), favorable apparent permeability ($P_{app(A\to B)}$ = 23 × 10^{-6} cm/s), and suitable aqueous solubility (34 μM). Thus, the δ-sultam subseries possessed favorable in vitro properties regardless of the stereochemistry at the 3-methyl or 6-phenyl substituents.

The (6*R*)-phenyl δ-sultam analogues **23**, **25**, **27**, and **29**, all of which possessed favorable in vitro CL_{hep} values, were progressed into single dose rat experiments to assess their in vivo PK profiles (Table 4). These δ-sultam analogues all possessed low-to-moderate in vivo clearance values (CL_p = 12−19 mL/min/kg), moderate volumes of distribution (V_d = 2.0−3.3 L/kg), and reasonable oral bioavailability values (*F*% = 36−99%). Overall, there was a very favorable in vitro/in vivo correlation (IVIVc) with these four analogues, with only 2-fold variability between the in vitro RLM CL_{hep} (Table 1) and rat in vivo CL_p values. Compound **27** possessed the most favorable in vivo profile in this set of analogues with low clearance (CL_p = 12 mL/min/kg), a modest volume of distribution (V_d = 3.3 L/kg), and reasonable oral bioavailability (*F*% = 55%). We also found that **27** did not inhibit the major CYP isoforms in vitro up to compound concentrations of 10 μM.[42]

We profiled **31** and the (6*R*)-phenyl δ-sultam analogues **23**, **25**, **26**, **27**, and **29** in a series of HEK-293 cell GAL4-ROR-LBD construct transcriptional reporter assays (Table 5). We profiled the three isoforms of human ROR (RORc, RORb, and RORa) by monitoring the suppression of their basal transcriptional activity in the absence of any exogenous agonist.[33] To assess the NR cellular selectivity of the potent RORc inverse agonists, we also tested these compounds in a small panel of cellular

Table 4. Single Dose Rat in Vivo PK Properties[a]

compd	CL_p[e] (mL/min/kg)	V_d[f] (L/kg)	C_{max}[g] (μM)	AUC (μM·h)	$t_{1/2}$ (h)	*F*%[h]
23[b]	13	2.9	0.6	3.9	3.3	74
25[c]	19	2.5	0.6	1.0	1.6	>99
27[d]	12	3.3	0.5	2.5	3.5	55
29[d]	15	2.0	0.4	1.3	1.6	36

[a]See the Supporting Information for experimental details associated with each assessment. Data reported are the means from the dosing cohorts (male Sprague−Dawley rats, *n* = 3/dose). [b]Dosed at 1.5 mg/kg po (75/25 solution of DMSO/H_2O) and 0.5 mg/kg iv (50/25/25 solution of DMSO/PEG400/saline). [c]Dosed at 1.5 mg/kg po (40/60 suspension of DMSO/MCT) and 0.5 mg/kg iv (28/50/22 solution of DMSO/PEG400/saline). [d]Dosed at 1.5 mg/kg po (37/63 suspension of DMSO/MCT) and 0.5 mg/kg iv (25/50/25 solution of DMSO/PEG400/saline). [e]Observed plasma clearance (CL_p). [f]Volume of distribution (V_d). [g]Maximum plasma concentration (C_{max}). [h]Oral bioavailability (*F*%) was calculated according to the equation: *F*% = (dose normalized AUC_{po})/(dose normalized AUC_{iv}). CL_p, V_d, and $t_{1/2}$ were derived from an iv study and C_{max}, AUC, and *F*% were derived from a po study.

reporter assays of human farnesoid X receptor (FXR), liver X receptor (LXR)-α, LXRβ, and pregnane X receptor (PXR) in both agonist mode (no agonist ligand added) and antagonist mode (using T0901317 [*N*-(2,2,2-trifluoroethyl)-*N*-[4-[2,2,2-trifluoro-1-hydroxy-1-(trifluoromethyl)ethyl]phenyl]-benzenesulfonamide] as an exogenous ligand).[33] Compound **31** was a selective RORc inverse agonist with >130-fold selectivity for RORc over the other NRs in our cell assay panel (Table 5). Compound **23** possessed moderate RORc inverse agonist potency in the cell assay (EC_{50} = 670 nM), with no notable activity against any of the other RORs or NRs in the small cell panel. We were encouraged by this initial outcome with **23** as the δ-sultam subseries did not impart any additional off-target activities over that previously observed with the tertiary sulfonamide series (e.g., **31**).

This initial observation was confirmed with compounds **25** (RORc EC_{50} = 46 nM) and **27** (RORc EC_{50} = 47 nM), as both compounds displayed 75-fold selectivity for RORc over the other ROR isoforms and >200-fold selectivity over the other NRs in the cell assay panel. Compound **29**, which was less potent in the RORc biochemical assay than **25** and **27**, displayed modest RORc cellular potency (EC_{50} = 480 nM). None of these compounds displayed agonist mode activity against the NRs in the small cell assay panel at concentrations up to 10 μM. Compound **27** was also profiled against a larger cell assay panel of 21 additional NRs,[43] where it displayed no dose-dependent agonist or antagonist activity against the NRs at concentrations up to 10 μM, further demonstrating the high selectivity of **27** for RORc (>200-fold).

DOI: 10.1021/acs.jmedchem.5b00597
J. Med. Chem. XXXX, XXX, XXX−XXX

Table 5. RORc Potency and Selectivity Profiles in GAL4 Human Transcription Assays[a]

compd	RORc cell EC_{50} (μM) [%max]	RORb cell EC_{50} (μM) [%max]	RORa cell EC_{50} (μM) [%max]	FXR cell EC_{50} (μM) [%max]	LXRα cell EC_{50} (μM) [%max]	LXRβ cell EC_{50} (μM) [%max]	PXR cell EC_{50} (μM) [%max]
31	0.073 [97][b]	16.7 [64][b]	>20 [43][b]	>10 [−6]	>10 [3]	>10 [−10]	>10 [−70]
23	0.67 [93]	>10 [51]	>10 [44]	>10 [37]	>10 [−30]	>10 [13]	>10 [34]
25	0.046 [96]	9.9 [55]	>10 [25]	>10 [−10]	>10 [−20]	>10 [0]	>10 [8]
26	0.11 [94]	0.092 [94]	6.1 [75]	>10 [4]	>10 [−10]	>10 [1]	>10 [−40]
27	0.047 [99]	3.5 [83]	5.4 [74]	>10 [9]	>10 [−20]	>10 [−10]	>10 [15]
29	0.48 [97]	3.3 [86]	7.3 [69]	>10 [22]	>10 [−20]	>10 [−5]	>10 [−150]

[a]All assays were conducted in HEK293 cells transiently transfected with GAL4-NR-luciferase plasmids. These NR assays monitored the suppression of basal transcriptional activities (e.g., no agonist ligand was applied, only test compound was added), an outcome consistent with inverse agonist activity of the ligands.[33] All EC_{50} values are reported as means (all standard deviations were <54% of the mean EC_{50} values) for ≥4 separate titrations for the RORs and ≥2 separate titrations for the LXRs, FXR, and PXR; the maximum percent inhibition "%max" was observed at the highest test concentration of 10 μM, unless otherwise noted, and the %max values are reported as means (all standard deviations were <17% of the mean %max values). In this table, positive %max indicates suppression of basal reporter signal, whereas negative %max denotes increased transcription relative to DMSO-treated cells. [b]For this compound, the %max represents inhibition at the highest test concentration of 20 μM.

Table 6. Potency in Human IL-17 and IFNγ Production Assays[a]

compd	IL-17AA EC_{50} (μM) [%max]	IFNγ EC_{50} (μM) [%max]	CTG EC_{50} (μM) [%max]
31	0.36 [79]	>20 [45]	>20 [18]
25	0.79 [69]	>20 [6]	>20 [1]
27	0.45 [82]	>20 [45]	>20 [23]

[a]All assay EC_{50} values are reported as means (all standard deviations were <77% of the mean EC_{50} values) for ≥3 separate titrations; the maximum percent inhibition "%max" was observed at the highest test concentration of 20 μM and are reported as means (all standard deviations were <10% of the mean %max value). All assays were conducted using peripheral blood mononuclear cells (PBMCs) isolated from human whole blood.[33] Interferon gamma (IFNγ) and CellTiter-Glo (CTG) readouts were obtained to monitor for inhibition of non-T_H17 cell cytokine production as well as adverse off-target effects on cell physiology, respectively.[33]

Compound **26** was profiled in our NR cell assay panel (Table 5), and it possessed moderate RORc and RORb inverse agonist activities (RORc EC_{50} = 110 nM, RORb EC_{50} = 92 nM).[44] To our knowledge, this is the first reported ligand with nearly equivalent RORb and RORc inverse agonist cellular potencies.[45] The selectivity profile of **26** was a stark contrast to the highly selective RORc inverse agonist profile of **27**, given that these two compounds are nearly identical except for their differing stereochemistry at the 6-phenyl group on the δ-sultam ring. It is our hypothesis that the conformation of the (6*S*)-phenyl δ-sultam ring in **26** may play a role in its enhanced RORb activity, but we do not have any crystallographic evidence to support this theory.

On the basis of their favorable RORc cell potency and selectivity values, compounds **31**, **25**, and **27** were progressed into human PBMC cytokine production assays[33] to assess their abilities to inhibit the T cell receptor-dependent production of IL-17 (Table 6). The IL-17 family contains six members, IL17-A, -B, -C, -D, -E, and -F, and these family members can exist as homodimers and heterodimers.[19] The forms of IL-17 most relevant to T helper (T_H)-17-mediated inflammatory diseases are IL-17AA, -AF, and -FF.[19] Therefore, we chose to monitor the production of IL-17AA in our human PBMC assay. Compounds **31**, **25**, and **27** displayed modest inhibition of IL-17AA production in the human PBMC assay (EC_{50} = 350, 650, and 370 nM, respectively). It is also noteworthy that none of the compounds showed any activity in the interferon (IFN)-γ or CellTiter-Glo (CTG) assays, demonstrating that the compounds were not indiscriminately suppressing cytokine production nor were they grossly cytotoxic. We were encouraged that **25** and **27** displayed comparable human PBMC potencies to **31**, further demonstrating that the δ-sultam subseries could achieve similar potency to the tertiary sulfonamide series of RORc inverse agonists.[23,25,26]

Before assessing whether our molecules possessed favorable activity in vivo, we established in vitro murine cell assays to complement the human cell data we collected. Human NR1F3 (RORc) and murine NR1F3 (RORγ) exist in two distinct splice variants: RORc1/RORc2 for humans and RORγ1/RORγt for mice.[1,19,46,47] The splice variants within each species differ only in the lengths of their *N*-terminal sequences. The LBDs of the slice variants within each species share identical sequence homology. Our δ-sultam RORc inverse agonists cannot discern one RORc splice variant over another (e.g., RORc1 vs RORc2) because they were designed to target the human RORc-LBD. Murine RORγ and human RORc share an 88% sequence homology.[48] Because of the sequence difference between human and murine NR1F3, we assessed our potent and selective human RORc inverse agonist **27** in murine in vitro IL-17 assays. This approach ensured that **27** could adequately suppress the production of IL-17 in mouse cells prior to progressing into murine in vivo models.

Because **27** provided an appealing profile in the human PBMC assay, we explored its ability to inhibit IL-17 production in various murine cell-based assays. To do so, we generated mouse T_H17 cells from female C57BL/6J mice using two different conditions: (1) a mixture of IL-1β, IL-6, and IL-23, and (2) a combination of transforming growth factor (TGF)-β and IL-6. In the presence of IL-1β, IL-6, and IL-23, murine T_H17 cells are defined as "pathogenic" cells.[49] In addition to producing IL-17, pathogenic T_H17 cells also produce IFNγ and are involved in autoimmunity and inflammation. In the presence of the TGF-β and IL-6 conditions, murine T_H17 cells coexpress IL-10 and are defined as "suppressive" cells.[49] Pathogenic and suppressive T_H17 cells produce three IL-17 subtypes: IL-17AA, -AF, and -FF, which all signal through the same receptor (IL-17RA·IL-17RC). As shown in Table 7, murine $CD4^+$ T cells produce IL-17AF at a higher concentration than IL-17AA or -FF, regardless of the stimulus. $CD4^+$

DOI: 10.1021/acs.jmedchem.5b00597
J. Med. Chem. XXXX, XXX, XXX−XXX

Table 7. Murine IL-17 Production Assay Results with 27[a]

	CD4+ T cells						splenocytes		
	IL-1β/IL-6/IL-23 stimulus			TGF-β/IL-6 stimulus			IL-1β/IL-6/IL-23 stimulus		
	IL-17 AA	IL-17 AF	IL-17 FF	IL-17 AA	IL-17 AF	IL-17 FF	IL-17 AA	IL-17 AF	IL-17 FF
max IL-17 production[b] (ng/mL)	8500	49000	4500	16000	36000	2600	870	3700	ND
EC_{50} of 27[c] (μM)	0.45	0.95	0.47	1.8	0.53	0.27	1.1	3.6	
%max inhibition with 27 at 10 μM	87	85	99	99	96	90	95	94	

[a]See the Supporting Information for the murine IL-17 production assay protocols. ND = not detected. [b]Experiments conducted in the absence of 27 to determine the maximum production of murine IL-17 under various conditions. [c]All EC_{50} values are reported as means (all standard deviations were <15% of the mean EC_{50} values) for ≥2 separate titrations using cells from female C57BL/6J mice.

T cells are not the only source of IL-17. In the presence of IL-1β, IL-6, and IL-23, murine innate lymphoid cells (ILCs) produce IL-17 as well.[50] To further explore the production of IL-17 by ILCs, we treated female C57BL/6J mouse splenocytes with a mixture of IL-1β, IL-6, and IL-23 (Table 7). Under these conditions, IL-17AF was produced at higher concentration than IL-17AA, and IL-17FF production was undetectable by ELISA. We were pleased to see that **27** inhibited the production of all three IL-17 subtypes in murine $CD4^+$ T cells, regardless of stimulus (EC_{50} = 0.27−1.8 μM, Table 7). Compound **27** also inhibited the production of IL-17AA and -AF by ILCs in the murine splenocyte assay (EC_{50} = 1.1−3.6 μM).

After observing that **27** inhibited IL-17 production in vitro in human PBMC and murine cellular assays, its attractive selectivity profile and metabolic stability prompted us to investigate its ability to suppress IL-17 production in vivo in a PK/PD model. Although **27** had favorable HLM, RLM, and in vivo rat PK clearance values, the mouse liver microsome (MLM) clearance was moderate-to-high (CL_{hep} = 60 mL/min/kg). A single dose mouse PK study (Table 8) where **27** was orally

Table 8. High Dose Mouse in Vivo Oral PK Properties of 27[a]

compd	pretreatment with 1-ABT[b]	AUC (μM·h)	C_{max}[c] (μM)
27	no	58.7	12.3
27	yes	371	32.8

[a]Compound dosed at 100 mg/kg po (MCT suspension). See the Supporting Information for experimental details associated with each assessment. Data reported are the means from the dosing cohorts (female CD-1 mice, n = 4/dose). [b]Mice treated with 15 mg/kg ip of 1-ABT 2 h prior to dosing with compound. [c]Maximum plasma concentration (C_{max}) from a po study.

administered as a 100 mg/kg 0.2% (v/v) methylcellulose Tween 80 (MCT) suspension resulted in low exposure (AUC = 58.7 μM·h, C_{max} = 12.3 μM), further corroborating the MLM clearance value. Compound **27** exhibited similar PPB values (Table 3) across human, rat, and mouse (murine $\%PPB_{(bound)}$ = 96%), thus the low exposure in mouse cannot be attributed to differences in PPB values.[51] In an effort to improve the murine in vivo oral exposure of **27**, mice in the PK study were treated with 1-aminobenzotriazole (1-ABT) 2 h prior to dosing with **27** to disrupt the CYP metabolism of **27**.[52] Thus, oral administration of **27** as a 100 mg/kg MCT suspension to mice pretreated with 1-ABT provided a substantial increase in exposure (AUC = 371 μM·h, C_{max} = 32.8 μM). This approach was then applied to a mouse PK/PD study to increase the exposure of **27**.

For the PK/PD study, mice were treated with 1-ABT 2 h prior to dosing with **27** (see Supporting Information for the details of the mouse IL-17 PK/PD experiment). Compound **27** was then dosed orally as an MCT suspension at 3, 10, 30, 100, and 200 mg/kg. The study animals were stimulated 1 h later with iv administration of mouse IL-1β and IL-23 recombinant protein to spur the production of IL-17.[53] Three hours later, blood was drawn and systemic levels of serum IL-17FF were measured by cytokine ELISA, and the total plasma concentrations of **27** were also determined at this time point. Inhibition of the IL-17 pathway was observed all for doses of **27** (Figure 2a), with dose-proportional inhibition of IL-17 and a maximal PD response (89% inhibition) at the 200 mg/kg dose. Overall, the PK/PD relationship suggested that a significant attenuation of IL-17FF production could be achieved at doses of 30, 100, and 200 mg/kg. All doses achieved dose-proportional increases in exposure as assessed by the total plasma concentration of **27** at the end of the study (Figure 2b). Anti-p40 antibody, which neutralizes IL-12 and IL-23 cytokines, was used as a positive control and resulted in near complete (>99%) inhibition of IL-17FF production. An isotype control antigen recognizing ragweed was used as the negative control in this study, and it matched the inhibition achieved with the vehicle control (PBS).

All doses of **27** in the mouse IL-17 PK/PD study resulted in total plasma concentrations of **27** (Figure 2b) that exceeded the in vitro IL-17FF EC_{50} value in the murine $CD4^+$ T cell assay conducted under IL-1β, IL-6, and IL-23 conditions (EC_{50} = 0.47 μM, Table 7).[54] However, **27** only demonstrated significant inhibition of IL-17FF production in the PK/PD study at total plasma concentrations ≥8 μM (e.g., 30, 100, and 200 mg/kg doses, Figure 2a). The total plasma concentration of ≥8 μM corresponded to a free-drug concentration of ≥0.32 μM in mice. This result suggested that a total drug plasma concentration in excess of the murine $CD4^+$ T cell EC_{50} assay value may be required to demonstrate in vivo inhibition of IL-17FF production. This hypothesis correlates with a total plasma concentration coverage of the EC_{90} value of **27** in the murine $CD4^+$ T cell assay conducted under IL-1β, IL-6, and IL-23 conditions (EC_{90} = 7 μM), as was achieved at the 30, 100, and 200 mg/kg doses in the IL-17 PK/PD study (Figure 2b). In sum, these results suggest that inhibition of murine IL-17FF production in vivo may require a total plasma drug concentration that covers the in vitro murine IL-17FF production EC_{90} assay value. It is unknown if this same relationship will hold true for the in vivo suppression of human IL-17 production with selective RORc inverse agonists.

CONCLUSION

In conclusion, we have evolved a previously disclosed tertiary sulfonamide series of RORc inverse agonists into a related yet distinct δ-sultam series. The (6*R*)-phenyl δ-sultam analogues demonstrated favorable HLM and RLM profiles, a good IVIVc,

DOI: 10.1021/acs.jmedchem.5b00597
J. Med. Chem. XXXX, XXX, XXX−XXX

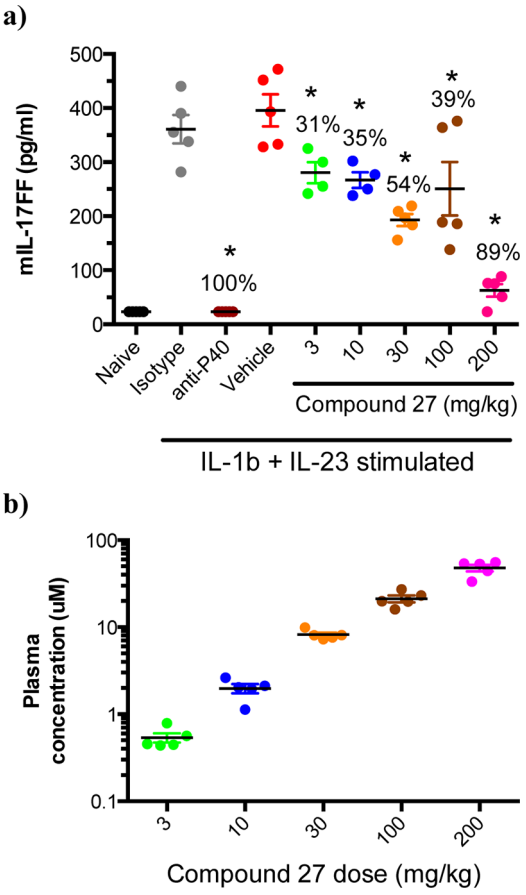

Figure 2. Mouse IL-17 PK/PD results for **27**. Six-to-eight week old female C57BL/6J mice were administered 15 mg/kg of 1-ABT (MCT suspension) 2 h prior to compound administration. Compound **27** was dosed po (MCT suspension) at five different doses (3, 10, 30, 100, 200 mg/kg) with five mice per dose cohort. One hour after **27** was dosed, the mice were stimulated with 300 ng of IL-1β and 100 ng of IL-23. Blood was collected 3 h poststimulation and was analyzed for the serum IL-17FF concentration by ELISA (means ± SEM) and the plasma concentration of **27** (means ± SEM). An isotype control antigen recognizing ragweed was used as the negative control and anti-p40 antibody was used as a positive control in the study. A Dunnett's test comparison of the IL-1β + IL-23 isotype control animals versus the animals treated with **27** provided the following statistical *p*-value: $^{*}p < 0.05$.

and potent RORc inverse agonist activity in biochemical and cellular assays. Conversely, the (6*S*)-phenyl δ-sultam analogues demonstrated moderate-to-high CL_{hep} values in HLM and RLM studies and poor RORc inverse agonist activity. It was also notable that one of the (6*S*)-phenyl δ-sultam analogues (**26**) exhibited selectivity for RORb and RORc. The most advanced (6*R*)-phenyl δ-sultam compound (**27**) possessed favorable RORc cellular potencies, with 75-fold selectivity for RORc over other ROR family members and >200-fold selectivity over 25 additional nuclear receptors in a cell assay suite. The favorable potency, selectivity, in vitro ADME properties, in vivo PK, and dose-dependent inhibition of IL-17 in a PK/PD model support the evaluation of **27** in preclinical studies.

EXPERIMENTAL SECTION

Chemistry. *General.* All chemicals were purchased from commercial suppliers and used as received. Flash chromatography was carried out with prepacked SiO_2 cartridges from either ISCO or SiliCycle on an ISCO CombiFlash chromatography system using gradient elution. Optical rotation data were recorded on a Rudolph Research Analytical Autopol V polarimeter. The reported specific rotations were recorded at the designated temperatures, light source wavelengths, concentrations (g/100 mL), and in the designated solvents. NMR spectra were recorded on a Bruker Avance 400, Bruker DPX 400M, or Bruker Avance III 400 or 500 NMR spectrometers and internally referenced to $SiMe_4$. The following abbreviations are used: br = broad signal, s = singlet, d = doublet, dd = doublet of doublets, t = triplet, q = quartet, and m = multiplet. Preparative HPLC was performed on a Polaris C_{18} column (50 mm × 21 mm, 5 μm), a Waters Sunfire OBD Phenomenex Luna Phenyl Hexyl column (150 mm × 19 mm), or a Waters Xbridge Phenyl column (150 mm × 19 mm), eluting with mixtures of H_2O/CH_3CN or H_2O/CH_3OH, optionally containing a modifier (0.1% v/v formic acid or 10 mM ammonium bicarbonate). Stereoisomers of the final products were separated on a PIC-100 SFC system using CO_2/MeOH + 0.1% v/v NH_4OH mobile phases and a Chiralpak AD column (21 mm × 150 mm, 5 μm). Low-resolution mass spectra were recorded on a Sciex 15 mass spectrometer in ES^+ mode, a Micromass ZQ single quadrapole LC-MS in ES^+, ES^- mode, or a Quattro Micro LC-MS-MS in ES^+, ES^- mode. All final compounds were purified to >95% chemical and optical purity, as assayed by either: (a) HPLC (Waters Acquity UPLC column 21 mm × 50 mm, 1.7 μm) with gradient of 0−90% CH_3CN (containing 0.04% v/v TFA) in 0.1% v/v aqueous TFA, with UV detection at λ = 254 and 210 nm as well as CAD detection with an ESA Corona detector, (b) HPLC (Phenomenex Luna C18 (2) column 4.6 mm × 100 mm, 5 μm) with gradient of 5−95% CH_3CN in H_2O (with 0.1% v/v formic acid in each mobile phase), with UV DAD detection between λ = 210 and 400 nm, (c) HPLC (Waters Xterra MS C18 column 4.6 mm × 100 mm, 5 μm) with gradient of 5−95% CH_3CN in H_2O (with 10 mM ammonium bicarbonate in the aqueous mobile phase), with UV DAD detection between λ = 210 and 400 nm, (d) HPLC (Supelco, Ascentis Express C18 or Hichrom Halo C18 column 4.6 mm × 150 mm, 2.7 μm) with gradient of 4−100% CH_3CN in H_2O (with 0.1% v/v formic acid in each mobile phase), with UV DAD detection between λ = 210 and 400 nm, or (e) HPLC (Phenomenex, Gemini NX C18 column 4.6 mm × 150 mm, 3 μm) with gradient of 4.5−100% CH_3CN in H_2O (with 10 mM ammonium bicarbonate in the aqueous mobile phase), with UV DAD detection between λ = 210 and 400 nm.

The synthesis of compound **1** was described previously.[25]

*N-(2-Cyanopropan-2-yl)-1-phenylmethanesulfonamide (**5**).* To a solution of 2-amino-2-methylpropanenitrile (**4**, 0.12 g, 1.4 mmol) in DCM (1.5 mL) was added *N,N*-di-*iso*-propylethylamine (0.29 mL, 1.7 mmol), followed by phenylmethanesulfonyl chloride (0.32 g, 1.7 mmol). The reaction was stirred at ambient temperature for 16 h. The mixture was diluted with DCM (10 mL), washed with water (5 mL) and brine (5 mL), dried over $MgSO_4$, filtered, and purified by silica gel column chromatography (0−100% EtOAc in heptane) to provide the title compound (0.15 g, 46% yield). ^1H NMR (400 MHz, $CDCl_3$) δ 7.51−7.43 (m, 2H), 7.43−7.36 (m, 3H), 4.48 (s, 2H), 4.27 (s, 1H), 1.68 (s, 6H). LCMS ES^+ m/z = 256 $[M + NH_4]^+$.

*N-(4-(4-Acetylpiperazin-1-yl)benzyl)-5-phenyl-4-amino-3,3-dimethyl-2,3-dihydroisothiazole-1,1-dioxide (**6**).* *Step 1.* To a solution *N*-(2-cyanopropan-2-yl)-1-phenylmethanesulfonamide (**5**, 0.16 g, 0.65 mmol) in DMA (3 mL) was added NaH (60% in mineral oil, 31 mg, 0.78 mmol), and the reaction was stirred at ambient temperature for 30 min. 1-Bromo-4-(bromomethyl)benzene (0.18 g, 0.72 mmol) was added to the reaction and the mixture was stirred at 75 °C for 16 h. The reaction was quenched with water (1 mL), diluted with EtOAc (10 mL), washed with water (5 mL) and brine (5 mL), dried over $MgSO_4$, filtered, concentrated, and purified by silica gel column chromatography (0−100% EtOAc in heptane) to provide the *N*-benzylated intermediate (91 mg) that was carried on to the next step as the crude intermediate. LCMS ES^+ m/z = 408 $[M + H]^+$.

Step 2. A vial was charged with the *N*-benzylated intermediate from step 1 (91 mg, 0.22 mmol), chloro-(2-dicyclohexylphosphino-2′,6′-di-*iso*-propoxy-1,1′-biphenyl)[2-(2-aminoethyl)phenyl]palladium(II)

DOI: 10.1021/acs.jmedchem.5b00597
J. Med. Chem. XXXX, XXX, XXX−XXX

methyl-*tert*-butyl ether adduct (16 mg, 0.022 mmol), 2-dicyclohexylphosphino-2′,6′-di-*iso*-propoxybiphenyl (11 mg, 0.022 mmol), and sodium *tert*-butoxide (33 mg, 0.33 mmol) and purged with nitrogen gas for 2 min. A solution of *N*-acetylpiperazine (43 mg, 0.33 mmol) in 1,4-dioxane (1 mL) was added to the reaction, and the mixture was stirred at 100 °C for 16 h. The reaction was filtered through diatomaceous earth, concentrated under reduced pressure, and purified by reverse-phase HPLC to give provide the title compound (43 mg, 14% yield over 2 steps). ^{1}H NMR (400 MHz, DMSO-d_6) δ 7.49 (d, J = 7.2 Hz, 2H), 7.41 (t, J = 7.7 Hz, 2H), 7.29 (dd, J = 15.9, 8.1 Hz, 3H), 6.92 (d, J = 8.7 Hz, 2H), 6.41 (s, 2H), 4.20 (s, 2H), 3.57 (s, 4H), 3.18−3.11 (m, 2H), 3.11−3.02 (m, 2H), 2.03 (s, 3H), 1.32 (s, 6H). LCMS ES$^+$ m/z = 455 [M + H]$^+$.

General Procedure A: Formation of Sultam Rings ***12−16***. The sultam rings were prepared in a multistep process according to the literature procedure of Lee et al.[30]

General Procedure B: Formation of Products ***17−21***. *Step 1*. The sultam rings obtained by general procedure A (**12−16**, 1.0 equiv) were combined with 4-bromo-1-(bromomethyl)-2-fluorobenzene (1.1 equiv) and DMF (0.2 M) at 0 °C. Sodium hydride (60% in mineral oil, 1.2 equiv) was added to the reaction portionwise. The resultant mixture was stirred at ambient temperature for 2 h. Water was added, and the reaction was diluted with EtOAc, washed with brine, dried over $MgSO_4$, filtered, and purified by silica gel column chromatography (0−60% EtOAc/heptane) to provide the *N*-benzylated intermediates to be used directly in the next step.

Step 2. The *N*-benzylated intermediates obtained in step 1 (1.0 equiv) were combined with $Pd(OAc)_2$ (0.05 equiv), 2-dicyclohexylphosphine-2′,6′-di-*iso*-propoxy-1,1′-biphenyl (0.10 equiv), and Cs_2CO_3 (1.5 equiv) in a vial and purged with nitrogen gas for 2 min. 1,4-Dioxane (0.3 M) and *N*-acetylpiperazine (1.5 equiv) were added to the vial, and the reaction was stirred at 80 °C for 2−16 h. The reaction was filtered through diatomaceous earth, concentrated under reduced pressure, and purified by reverse-phase HPLC to provide the title compounds.

5-Phenylisothiazolidine 1,1-dioxide ***(12)***. 2-Bromoethanamine hydrobromide (**7**, 6.4 g, 32 mmol) was subjected to a multistep process according to the literature procedure of Lee et al.[30] to produce the title compound (2.6 g, 42% yield over 2 steps). ^{1}H NMR (300 MHz, $CDCl_3$) δ 7.45−7.26 (m, 5H), 4.42 (m, 1H), 4.28 (m, 1H), 3.54−3.49 (m, 2H), 2.85−2.72 (m, 2H). LCMS ES$^+$ m/z = 220 [M + Na]$^+$.

6-Phenyl-1,2-thiazinane-1,1-dioxide ***(13)***. 3-Bromoproan-1-amine hydrobromide (**8**, 2.2 g, 10 mmol) was subjected to a multistep process according to the literature procedure of Lee et al.[30] to produce the title compound (1.2 g, 59% yield over 2 steps). ^{1}H NMR (300 MHz, DMSO-d_6) δ 7.40−7.35 (m, 5H), 6.98 (m, 1H), 4.12 (m, 1H), 3.26−3.20 (m, 2H), 2.40−2.30 (m, 1H), 2.16−2.12 (m, 1H), 1.77−1.65 (m, 2H). LCMS ES$^+$ m/z = 234 [M + Na]$^+$.

(3R)-3-Methyl-6-phenyl-1,2-thiazinane 1,1-dioxide ***(14)***. (*R*)-3-Aminobutan-1-ol[29] (**9**, 1.0 g, 11 mmol) was subjected to general procedure A to produce the title compound (0.83 g, 33% yield over 3 steps). ^{1}H NMR (400 MHz, DMSO-d_6, reported as a 3:1 mixture of diastereomers) δ 7.52−7.30 (m, 5H), 7.10 (d, J = 5.9 Hz, 0.25H), 6.79 (d, J = 9.8 Hz, 0.75H), 4.18 (dd, J = 9.8, 3.9 Hz, 0.25H), 4.02 (dd, J = 12.8, 3.5 Hz, 0.75H), 3.65−3.52 (m, 0.25H), 3.52−3.34 (m, 0.75H), 2.47−2.26 (m, 1H), 2.24−2.04 (m, 1H), 1.90−1.76 (m, 1H), 1.69−1.54 (m, 0.25H), 1.55−1.34 (m, 0.75H), 1.31 (d, J = 7.1 Hz, 0.75H), 1.15 (d, J = 6.6 Hz, 2.25H). LCMS ES$^+$ m/z = 226 [M + H]$^+$.

(3S)-3-Methyl-6-phenyl-1,2-thiazinane 1,1-dioxide ***(15)***. (*S*)-3-Aminobutan-1-ol[29] (**10**, 7.5 g, 84 mmol) was subjected to general procedure A to produce the title compound (4.0 g, 21% yield over 3 steps). ^{1}H NMR (400 MHz, DMSO-d_6, reported as a 4:1 mixture of diastereomers) δ 7.50−7.31 (m, 5H), 7.09 (d, J = 5.5 Hz, 0.2H), 6.78 (d, J = 9.0 Hz, 0.8H), 4.18 (dd, J = 9.8, 4.0 Hz, 0.2H), 4.02 (dd, J = 12.8, 3.5 Hz, 0.8H), 3.64−3.52 (m, 0.2H), 3.49−3.37 (m, 0.8H), 2.46−2.29 (m, 1H), 2.24−2.08 (m, 1H), 1.91−1.76 (m, 1H), 1.66−1.55 (m, 0.2H), 1.53−1.38 (m, 0.8H), 1.31 (d, J = 7.1 Hz, 0.6H), 1.15 (d, J = 6.6 Hz, 2.4H). LCMS ES$^+$ m/z = 226 [M + H]$^+$.

3,3-Dimethyl-6-phenyl-1,2-thiazinane 1,1-dioxide ***(16)***. 3-Amino-3-methylbutan-1-ol (**11**) (2.0 g, 19 mmol) was subjected to general procedure A to produce the title compound (1.5 g, 33% yield over 3 steps). ^{1}H NMR (400 MHz, DMSO-d_6) δ 7.52−7.25 (m, 5H), 6.78 (s, 1H), 4.03 (dd, J = 12.8, 3.3 Hz, 1H), 2.63−2.52 (m, 1H), 2.15−2.02 (m, 1H), 1.76−1.67 (m, 2H), 1.36 (s, 3H), 1.21 (s, 3H). LCMS ES$^+$ m/z = 240 [M + H]$^+$.

1-{4-[4-(1,1-Dioxo-5-phenyl-isothiazolidin-2-ylmethyl)-3-fluoro-phenyl]-piperazin-1-yl}-ethanone ***(17)***. Compound **12** (0.15 g, 0.76 mmol) was subjected to general procedure B to provide the title compound (53 mg, 16% yield over 2 steps). ^{1}H NMR (400 MHz, DMSO-d_6) δ 7.52−7.35 (m, 5H), 7.26 (t, J = 8.6 Hz, 1H), 6.79 (d, J = 11.0 Hz, 2H), 4.65−4.52 (m, 1H), 4.20 (d, J = 14.5 Hz, 1H), 4.06 (d, J = 14.4 Hz, 1H), 3.64−3.50 (m, 4H), 3.29−3.08 (m, 6H), 2.63−2.52 (m, 1H), 2.49−2.42 (m, 1H), 2.04 (s, 3H). LCMS ES$^+$ m/z = 432 [M + H]$^+$.

1-{4-[4-(1,1-Dioxo-6-phenyl-[1,2]thiazinan-2-ylmethyl)-3-fluoro-phenyl]-piperazin-1-yl}-ethanone ***(18)***. Compound **13** (0.30 g, 1.4 mmol) was subjected to general procedure B to provide the title compound (0.39 g, 62% yield over 2 steps). ^{1}H NMR (400 MHz, DMSO-d_6) δ 7.49−7.31 (m, 5H), 7.26 (t, J = 8.8 Hz, 1H), 6.86−6.73 (m, 2H), 4.49 (dd, J = 12.6, 3.2 Hz, 1H), 4.35 (q, J = 14.4 Hz, 2H), 3.63−3.51 (m, 4H), 3.46 (t, J = 12.9 Hz, 1H), 3.28−3.19 (m, 2H), 3.19−3.04 (m, 3H), 2.48−2.35 (m, 1H), 2.22−2.07 (m, 1H), 2.04 (s, 3H), 2.01−1.87 (m, 1H), 1.72−1.49 (m, 1H). LCMS ES$^+$ m/z = 446 [M + H]$^+$.

1-(4-(3-Fluoro-4-(((3R)-3-methyl-1,1-dioxido-6-phenyl-1,2-thiazinan-2-yl)methyl)phenyl)piperazin-1-yl)ethanone ***(19)***. Compound **14** (0.15 g, 0.67 mmol) was subjected to general procedure B to produce the title compound (0.23 g, 73% yield over 2 steps). This compound was carried on directly to the next step and not characterized.

1-(4-(3-Fluoro-4-(((3S)-3-methyl-1,1-dioxido-6-phenyl-1,2-thiazinan-2-yl)methyl)phenyl)piperazin-1-yl)ethanone ***(20)***. Compound **15** (0.68 g, 3.0 mmol) was subjected to general procedure B to produce the title compound (0.92 g, 67% yield over 2 steps). This compound was carried on directly to the next step and not characterized.

1-(4-(4-((3,3-Dimethyl-1,1-dioxido-6-phenyl-1,2-thiazinan-2-yl)-methyl)-3-fluorophenyl)piperazin-1-yl)ethanone ***(21)***. Compound **16** (0.15 g, 0.63 mmol) was subjected to general procedure B to produce the title compound (0.30 g, 50% yield over 2 steps). This compound was carried on directly to the next step and not characterized.

1-{4-[4-((S)-1,1-Dioxo-6-phenyl-[1,2]thiazinan-2-ylmethyl)-3-fluoro-phenyl]-piperazin-1-yl}-ethanone ***(22)***. Compound **18** (0.15 g, 0.34 mmol) was subjected to SFC purification to yield the title compound (50 mg, 33% yield). The absolute stereochemistry of the title compound was assigned by analogy to **23**. $[\alpha]_D^{23}$ −19° (c 0.18, CH_3OH). ^{1}H NMR (400 MHz, DMSO-d_6) δ 7.53−7.32 (m, 5H), 7.29−7.22 (m, 1H), 6.85−6.80 (m, 1H), 6.80−6.75 (m, 1H), 4.54−4.44 (m, 1H), 4.38 (d, J = 14.4 Hz, 1H), 4.32 (d, J = 14.3 Hz, 1H), 3.63−3.52 (m, 4H), 3.52−3.40 (m, 1H), 3.28−3.20 (m, 2H), 3.20−3.04 (m, 3H), 2.47−2.36 (m, 1H), 2.18−2.07 (m, 1H), 2.04 (s, 3H), 2.02−1.91 (m, 1H), 1.71−1.56 (m, 1H). LCMS ES$^+$ m/z = 446 [M + H]$^+$.

1-{4-[4-((R)-1,1-Dioxo-6-phenyl-[1,2]thiazinan-2-ylmethyl)-3-fluoro-phenyl]-piperazin-1-yl}-ethanone ***(23)***. Compound **18** (0.15 g, 0.34 mmol) was subjected to SFC purification to yield the title compound (75 mg, 50% yield). The absolute stereochemistry of the title compound was assigned by single-crystal X-ray analysis (see Supporting Information). $[\alpha]_D^{23}$ +18° (c 0.17, CH_3OH). ^{1}H NMR (400 MHz, DMSO-d_6) δ 7.49−7.32 (m, 5H), 7.30−7.21 (m, 1H), 6.84−6.80 (m, 1H), 6.80−6.75 (m, 1H), 4.55−4.44 (m, 1H), 4.38 (d, J = 14.2 Hz, 1H), 4.32 (d, J = 14.4 Hz, 1H), 3.60−3.52 (m, 4H), 3.52−3.40 (m, 1H), 3.26−3.19 (m, 2H), 3.19−3.04 (m, 3H), 2.48−2.36 (m, 1H), 2.18−2.06 (m, 1H), 2.04 (s, 3H), 2.01−1.92 (m, 1H), 1.69−1.57 (m, 1H). LCMS ES$^+$ m/z = 446 [M + H]$^+$.

1-{4-[3-Fluoro-4-((3R,6S)-3-methyl-1,1-dioxo-6-phenyl-[1,2]-thiazinan-2-ylmethyl)-phenyl]-piperazin-1-yl}-ethanone ***(24)***. Compound **19** (0.22 g, 0.48 mmol) was subjected to SFC purification to yield the title compound (53 mg, 24% yield). The absolute stereochemistry was assigned by NMR analysis.[31] $[\alpha]_D^{23}$ +28° (c 0.18, CH_3OH). ^{1}H NMR (400 MHz, DMSO-d_6) δ 7.49−7.43 (m, 2H), 7.43−7.29 (m, 4H), 6.81 (dd, J = 8.6, 2.1 Hz, 1H), 6.74 (d, J = 13.9 Hz, 1H),

DOI: 10.1021/acs.jmedchem.5b00597
J. Med. Chem. XXXX, XXX, XXX−XXX

4.47 (dd, J = 12.0, 3.0 Hz, 1H), 4.41 (d, J = 16.9 Hz, 1H), 4.28 (d, J = 17.1 Hz, 1H), 4.15−4.03 (m, 1H), 3.59−3.52 (m, 4H), 3.22−3.15 (m, 2H), 3.15−3.08 (m, 2H), 2.46−2.35 (m, 1H), 2.13−2.05 (m, 1H), 2.03 (s, 3H), 1.89−1.73 (m, 1H), 1.69−1.60 (m, 1H), 1.08 (d, J = 6.9 Hz, 3H). LCMS ES$^+$ m/z = 460 [M + H]$^+$.

*1-{4-[3-Fluoro-4-((3R,6R)-3-methyl-1,1-dioxo-6-phenyl-[1,2]-thiazinan-2-ylmethyl)-phenyl]-piperazin-1-yl}-ethanone (**25**).* Compound **19** (0.22 g, 0.48 mmol) was subjected to SFC purification to yield the title compound (23 mg, 10% yield). The absolute stereochemistry was assigned by NMR analysis.[31] $[\alpha]_D^{23}$ +50° (c 0.18, CH_3OH). ^{1}H NMR (400 MHz, DMSO-d_6) δ 7.48−7.43 (m, 2H), 7.43−7.33 (m, 3H), 7.29 (t, J = 8.9 Hz, 1H), 6.85−6.77 (m, 2H), 4.40 (dd, J = 12.4, 3.2 Hz, 1H), 4.37 (s, 2H), 3.60−3.51 (m, 5H), 3.26−3.19 (m, 2H), 3.19−3.13 (m, 2H), 2.79−2.64 (m, 1H), 2.15−1.99 (m, 5H), 1.66−1.57 (m, 1H), 1.34 (d, J = 7.2 Hz, 3H). LCMS ES$^+$ m/z = 460 [M + H]$^+$.

*1-{4-[3-Fluoro-4-((3S,6S)-3-methyl-1,1-dioxo-6-phenyl-[1,2]-thiazinan-2-ylmethyl)-phenyl]-piperazin-1-yl}-ethanone (**26**).* Compound **20** (0.21 g, 0.46 mmol) was subjected to SFC purification to yield the title compound (22 mg, 10% yield). The absolute stereochemistry was assigned by NMR analysis.[31] $[\alpha]_D^{23}$ −45° (c 0.17, CH_3OH). ^{1}H NMR (400 MHz, DMSO-d_6) δ 7.49−7.43 (m, 2H), 7.43−7.34 (m, 3H), 7.29 (t, J = 8.9 Hz, 1H), 6.87−6.74 (m, 2H), 4.40 (dd, J = 12.4, 3.2 Hz, 1H), 4.37 (s, 2H), 3.60−3.48 (m, 5H), 3.25−3.18 (m, 2H), 3.18−3.11 (m, 2H), 2.81−2.61 (m, 1H), 2.17−1.95 (m, 5H), 1.67−1.53 (m, 1H), 1.34 (d, J = 7.1 Hz, 3H). LCMS ES$^+$ m/z = 460 [M + H]$^+$.

*1-{4-[3-Fluoro-4-((3S,6R)-3-methyl-1,1-dioxo-6-phenyl-[1,2]-thiazinan-2-ylmethyl)-phenyl]-piperazin-1-yl}-ethanone (**27**).* Compound **20** (0.21 g, 0.46 mmol) was subjected to SFC purification to yield the title compound (50 mg, 24% yield). The absolute stereochemistry was assigned by NMR analysis[31] and further confirmed by single-crystal X-ray analysis (see Supporting Information). $[\alpha]_D^{23}$ −22° (c 0.17, CH_3OH). ^{1}H NMR (400 MHz, DMSO-d_6) δ 7.49−7.43 (m, 2H), 7.43−7.28 (m, 4H), 6.81 (dd, J = 8.6, 2.1 Hz, 1H), 6.74 (d, J = 13.9 Hz, 1H), 4.48 (dd, J = 12.0, 3.0 Hz, 1H), 4.41 (d, J = 16.9 Hz, 1H), 4.28 (d, J = 17.1 Hz, 1H), 4.18−4.00 (m, 1H), 3.63−3.51 (m, 4H), 3.26−3.15 (m, 2H), 3.15−3.02 (m, 2H), 2.48−2.39 (m, 1H), 2.15−2.05 (m, 1H), 2.03 (s, 3H), 1.92−1.71 (m, 1H), 1.71−1.60 (m, 1H), 1.08 (d, J = 6.8 Hz, 3H). LCMS ES$^+$ m/z = 460 [M + H]$^+$.

*(S)-1-(4-(4-((3,3-Dimethyl-1,1-dioxido-6-phenyl-1,2-thiazinan-2-yl)methyl)-3-fluorophenyl)piperazin-1-yl)ethanone (**28**).* Compound **21** (0.15 g, 0.31 mmol) was subjected to SFC purification to yield the title compound (57 mg, 38% yield). The stereochemistry of the 6-phenyl substituent was assigned based on the relative specific optical rotation, biochemical potency, and metabolic stability of the title compound in relation to stereoisomers **22**−**27**. $[\alpha]_D^{23}$ −89° (c 0.18, CH_3OH). ^{1}H NMR (400 MHz, DMSO-d_6) δ 7.54−7.35 (m, 6H), 6.86−6.78 (m, 1H), 6.78−6.66 (m, 1H), 4.58−4.47 (m, 1H), 4.43 (d, J = 17.4 Hz, 1H), 4.19 (d, J = 17.5 Hz, 1H), 3.61−3.51 (m, 4H), 3.24−3.16 (m, 2H), 3.16−3.07 (m, 2H), 2.77−2.58 (m, 1H), 2.17−2.07 (m, 1H), 2.04 (s, 3H), 2.01−1.92 (m, 1H), 1.86−1.75 (m, 1H), 1.42 (s, 3H), 1.14 (s, 3H). LCMS ES$^+$ m/z = 474 [M + H]$^+$.

*(R)-1-(4-(4-((3,3-Dimethyl-1,1-dioxido-6-phenyl-1,2-thiazinan-2-yl)methyl)-3-fluorophenyl)piperazin-1-yl)ethanone (**29**).* Compound **21** (0.15 g, 0.31 mmol) was subjected to SFC purification to yield the title compound (56 mg, 37% yield). The stereochemistry of the 6-phenyl substituent was assigned based on the relative specific optical rotation, biochemical potency, and metabolic stability of the title compound in relation to stereoisomers **22**−**27**. $[\alpha]_D^{23}$ +85° (c 0.18, CH_3OH). ^{1}H NMR (400 MHz, DMSO-d_6) δ 7.53−7.34 (m, 6H), 6.86−6.77 (m, 1H), 6.77−6.66 (m, 1H), 4.57−4.48 (m, 1H), 4.43 (d, J = 17.5 Hz, 1H), 4.19 (d, J = 17.5 Hz, 1H), 3.61−3.51 (m, 4H), 3.23−3.16 (m, 2H), 3.16−3.07 (m, 2H), 2.77−2.56 (m, 1H), 2.20−2.06 (m, 1H), 2.04 (s, 3H), 2.01−1.92 (m, 1H), 1.88−1.73 (m, 1H), 1.42 (s, 3H), 1.14 (s, 3H). LCMS ES$^+$ m/z = 474 [M + H]$^+$.

The syntheses of compounds **30**[25] and **31**[23] were described previously.

Biological Assay Protocols.[33] *RORc SRC1 Biochemical Assay.* Assays were carried out in 16 μL reaction volumes in black 384 Plus F Proxiplates (Perkin-Elmer 6008269). All assay components except test ligand were mixed in coregulator buffer D (Invitrogen PV4420) containing 5 mM DTT and added to the plate at twice their final concentrations in a volume of 8 μL. Test ligands at 2× the final concentration were then added to the wells in 8 μL of coregulator buffer D containing 5 mM DTT and 4% DMSO. Final incubations contained 1× coregulator buffer D, 5 mM DTT, test ligand, 2% DMSO, 50 nM biotinyl-CPSSHSSLTERKHKILHRLLQEGSPS (American Peptide Company; Vista, CA), 2 nM europium anti-GST (Cisbio 61GSTKLB), 12.5 nM streptavidin-D2 (Cisbio 610SADAB), 50 mM KF, and 10 nM of bacterially expressed human RORc ligand binding domain protein containing an N-terminal 6xHis-GST-tag and residues 241−486 of accession NP_001001523. Ten test ligand concentrations were tested in duplicate. After the reaction plates were incubated for 3 h in the dark at room temperature (22−23 °C), the plate was read on an EnVision plate reader (PerkinElmer) following the europium/D2 HTRF protocol (ex 320, em 615 and 665, 100 μs lag time, 100 flashes, 500 μs window). The time-resolved FRET signal at 665 nm was divided by that at 615 nm to generate the signal ratio of each well. The signal ratio of wells containing RORc and peptide, but no test ligand were averaged and set to 0% effect while the signal ratios of the blank wells containing coactivator peptide but no RORc are averaged and set to −100% effect.

RORc exhibits a basal (constitutive) signal in this assay and test ligands can increase or decrease the signal ratio from this basal level. RORc agonists increase the signal ratio in this assay, resulting in a positive % effect value. Inverse agonists decrease the signal ratio, resulting in a negative % effect value. The EC_{50} value was the concentration of test compound that provided half-maximal effect (increased or decreased assay signal) and was calculated by Genedata Screener software (Genedata; Basel, Switzerland) using the following equation

$$\%\ \text{effect} = S_0 + \{(S_{\text{inf}} - S_0)/[1 + (10^{\log EC_{50}}/10^c)^n]\} \quad (1)$$

where S_0 equals the activity level at zero concentration of test compound, S_{inf} is the activity level at infinite concentration of test compound, EC_{50} is the concentration at which the activity reaches 50% of the maximal effect, c is the concentration in logarithmic units corresponding to the values on the x-axis of the dose−response curve plot, and n is the Hill coefficient (the slope of the curve at the EC_{50}).

Cellular Nuclear Receptor (NR) Transcriptional Reporter Assays. Assays were carried out in 30 μL reaction volumes in black 384-well tissue culture-treated viewplates (Perkin-Elmer 6007460). Ten test ligand concentrations were tested in duplicate. The reporter assays for RORa, RORb, and RORc were carried out in the absence of any control agonist ligand (inverse agonist mode). The assays for the other NRs were run in the absence (agonist mode) and presence (antagonist mode) of T0901317 as a control agonist ligand. HEK293T cells were cultured in complete medium [DMEM (Gibco 31966) supplemented with 10% heat-inactivated fetal bovine serum (PAA Laboratories A15-252)]. On the day of the assay, the cells were transiently cotransfected in bulk, using 2.5 μL of Lipofectamine 2000 (Invitrogen 11668-019) per μg of DNA, with an expression vector for a GAL4 fusion protein of a human NR (FXR, LXRα, LXRβ, PXR, RORa, RORb, or RORc; 40 ng/well) subcloned into either pLenti (Invitrogen) or pFastBacMam,[56] a firefly luciferase expression vector under control of the yeast GAL4 promoter (pFrLuc-GAL4UAS, Stratagene; 40 ng/well), and a pcDNA3.1 (Invitrogen) expression vector into which the *Renilla* luciferase sequence had been subcloned to generate a vector, pcDNA3.1Ren.Luc (4 ng/well). Then 20 μL of transfected cells (20000 cells total) were plated per well into 384-well viewplates, and the plates were placed in a cell culture incubator. Five hours later, test ligand at 3× the final concentration was added in a 10 μL volume of complete medium containing 0.9% DMSO. The plates were kept for another 20 h in the cell culture incubator before the luciferase activity was measured using the Dual-Glo luciferase kit (Promega E2940). At that time, the plates were allowed to equilibrate to room temperature before 30 μL of firefly luciferase reagent was added to each well. Plates were shaken for 15 min before measuring the firefly luciferase signal on an EnVision plate reader using the

DOI: 10.1021/acs.jmedchem.5b00597
J. Med. Chem. XXXX, XXX, XXX−XXX

ultrasensitive luminescence protocol. Finally, 30 μL of Stop & Glo reagent was added per well to quench the firefly luciferase signal and allow detection of the *Renilla* luciferase signal.

Inverse Agonist Format. Transient transfection of RORa, RORb, and RORc generates a GAL4 reporter signal in the absence of any added control agonist ligand. This constitutive reporter signal from transfected cells incubated with complete medium containing 0.3% DMSO constituted the uninhibited 0% effect and was compared with cells that were not transfected which defined the −100% effect. The percent inhibition was calculated with respect to these limits and the data were fit to eq 1 to generate EC_{50} values. Compounds that decreased firefly luciferase expression below the constitutive signal were potential inverse agonists.

Agonist Format. Activation of the LXRα, LXRβ, FXR, and PXR reporter signal in transfected cells was measured by an increase in firefly luciferase expression induced by test compounds. Complete medium containing 3 μM of T0901317 [*N*-(2,2,2-trifluoroethyl)-*N*-[4-[2,2,2-trifluoro-1-hydroxy-1-(trifluoromethyl)ethyl]phenyl]-benzenesulfonamide] in 0.3% DMSO defined the 100% effect activation level, while the basal activity in the absence of T0901317 set the 0% effect level. The % effect values were calculated with respect to these limits, and EC_{50} values were calculated by fitting the % effect titration data to

$$\%\ \text{of control} = [(\text{test ligand cpm} - \text{NSB cpm}) / (\text{TB cpm} - \text{NSB cpm})] \times 100 \quad (2)$$

The concentration of test ligand that inhibited binding by 50% (e.g., the IC_{50}) was calculated using XLfit by plotting the % of control versus test ligand concentration and fitting the data to a sigmoidal inhibition curve equation

$$\%\ \text{of control} = 100/[1 + ([I]/IC_{50})^{\text{slope}}] \quad (3)$$

where [I] was the test ligand concentration. Compounds that increased firefly luciferase expression above the basal level were potential agonists of that NR. The fold activation by test compounds was calculated from the raw assay signal by dividing the relative luminescence units (RLU) value in the presence of test compound by the RLU in the absence of test compound.

Antagonist Format. Inhibition of agonist-induced activation of LXRα, LXRβ, FXR, and PXR was measured by a reduction in firefly luciferase expression in transfected cells by test compounds. Test compounds were added in the presence of a stimulus (EC_{80} concentration of T0901317) in complete medium containing 0.3% DMSO final concentration. The EC_{80} stimulus concentrations were 1.5, 0.75, 3, and 0.5 μM T0901317 for LXRα, LXRβ, FXR, and PXR, respectively, and defined the 100% effect level in this assay format. The basal signal in the absence of T0901317 defined the 0% effect level. The percent inhibition was calculated with respect to these limits and IC_{50} values were determined by fitting the data to eq 1. Compounds that decreased firefly luciferase expression below the T0901317-stimulated level were potential antagonists of that NR.

Nonspecific Activity. In addition to measuring the firefly luciferase signal due to the transfected NR, the potential impact of off-target activity was also measured in the same wells by monitoring the effect of test compounds on *Renilla* luciferase expression. Complete medium containing 0.3% DMSO defined the constitutive expression 100% effect signal level. The percent inhibition was calculated with respect to this control signal. Cells that have not been transfected showed negligible signal in this assay. Compounds that decreased *Renilla* luciferase expression below the 100% effect signal level may have potential off-target activities that could be responsible for nonspecific inhibition or activation of the firefly reporter signal. EC_{50} values were calculated using eq 1.

Human Peripheral Blood Mononuclear Cell (PBMC) IL-17, IFNγ, and Viability Assays. On the day of the assay, PBMCs were isolated from heparin-treated human whole blood obtained from the Genentech Research Employee Donation Program. In each assay run, blood from two or more donors was processed in parallel. First, 15 mL of Ficoll-Paque (GE Healthcare 17-1440-03) was added to Leucosep tubes (Greiner 227290) and centrifuged at 524*g* for 5 min at room temperature. Blood was then diluted in an equal volume of phosphate-buffered saline (PBS) and 35 mL of the resultant mixture was added to each Leucosep tube. Tubes were centrifuged at 930*g* for 20 min at room temperature, brake off. After centrifugation, the PBMCs were harvested and washed twice in a total volume of 50 mL of Roswell Park Memorial Institute (RPMI) medium and then centrifuged at 524*g* for 7 min at room temperature, brake on. PBMCs were suspended in assay medium [Yssel's T cell medium[57,58] (Gemini Bioproducts 400-102) plus 10% human serum (Gemini Bioproducts 100-512)] to 1.25 million cells per mL. On the day before the assay, 50 μL of a 10 μg/mL solution of anti-CD3 (BD Biosciences 555329) in PBS was added to test wells and stimulated control wells of a 96-well white/clear bottom polypropylene plate (Corning 3610). Wells to be used for nonstimulated controls received 50 μL of PBS only. Plates were incubated overnight at 4 °C. On the day of the assay, the anti-CD3-coated plates were washed 3 times with 200 μL of PBS using a Biotek ELx405 automated plate washer. Immediately after plate washing, 160 μL of isolated PBMCs were added to the central wells of the plate; the perimeter wells received 200 μL of assay medium to reduce evaporation. Next, test ligands at 10× their final concentration were added to the plate in 20 μL of RPMI containing 2% DMSO, whereas nonstimulated and stimulated control wells received only RPMI plus 2% DMSO. Finally, 20 μL of 10 μg/mL anti-CD28 (BD Biosciences 555725) in assay medium were added to test and stimulated control wells. Nonstimulated control wells received 20 μL of assay medium. Plates were placed in a humidified cell culture incubator. After 48 h, the plates were centrifuged at 524*g* for 5 min at room temperature. The supernatant fluids (100 μL per well) were transferred to a 96-well V-bottom polypropylene plate (Greiner 655201) and stored at −80 °C. To assess cell viability, 100 μL of CellTiter-Glo reagent (Promega G7572) was then added to the original cell plates, which were incubated for 10 min on a plate shaker. The assay signal in relative luminescence (RLU) was measured on an EnVision plate reader with a 0.1 s read time. The mean RLU values of the perimeter blank wells defined 0% of control, while the mean values from stimulated control wells defined 100% of control. The % of control values for wells containing test ligand were calculated using the RLU data and

$$\%\ \text{of control} = [(\text{test ligand} - \text{blank})/(\text{stimulated} - \text{blank})] \times 100 \quad (4)$$

EC_{50} values (concentration of test ligand that provides half-maximal inhibition) were calculated using eq 1.

Cytokine ELISAs. Sandwich ELISAs for IL-17 (R&D Systems DY317) and IFNγ (R&D Systems DY285) were performed on the thawed supernatants in 96-well half area clear polystyrene plates (Costar 3690) following the vendor's protocols. On the day before the ELISAs, 25 μL of capture antibody diluted 180× in PBS was added to the ELISA plates. The plates were incubated overnight at room temperature. On the day of the assay, the plates were washed 3 times on a Biotek ELx405 automated plate washer with 200 μL of wash buffer (PBS + 0.05% Tween-20). Immediately after washing, the plates were blocked with ELISA buffer (PBS + 1% BSA) and incubated for 1 h at room temperature on a plate shaker. During this blocking step, frozen supernatant samples were thawed for 1 h at room temperature. After incubation, ELISA plates were washed as before. Next, 25 μL of supernatant samples were diluted in an equal volume of ELISA buffer, while 25 μL of buffer blanks and 25 μL of serial dilutions of the respective cytokine standard prepared in ELISA buffer were added to their designated wells on the plate. Plates were incubated for 2 h at room temperature or overnight at 4 °C on a plate shaker. After incubation, plates were washed as before. Next, 25 μL of detection antibody diluted 180× in ELISA buffer was added to all wells of the plate and incubated for 1 h at room temperature on a plate shaker. Plates were washed and then 25 μL of streptavidin-HRP diluted 200× in ELISA buffer was added to all wells of the plate. Plates were incubated for 20 min at room temperature on a plate shaker. Following incubation, plates were again washed. Then 25 μL of 3,3′,5,5′-tetramethylbenzidine liquid substrate (Sigma T4444) was added to the

DOI: 10.1021/acs.jmedchem.5b00597
J. Med. Chem. XXXX, XXX, XXX−XXX

plates. The plates were incubated for 15 min on a plate shaker. Finally, 25 μL of 1 M phosphoric acid stop solution was added to all wells of the plate. The absorption at 450 nm was read using a Molecular Devices SPECTRAmax PLUS384 plate reader. The mean absorption values for nonstimulated controls defined 0% of control, while the mean values from stimulated controls wells defined 100% of control. The % of control in each test compound well was calculated using eq 4, and EC_{50} values were calculated using eq 1.

■ ASSOCIATED CONTENT

Supporting Information

Additional NMR data, assay protocols, and X-ray data (PDF, CSV) can be found in the Supporting Information. The Supporting Information is available free of charge on the ACS Publications website at DOI: 10.1021/acs.jmedchem.5b00597.

Accession Codes

PDB 4WQP was discussed in this manuscript.

■ AUTHOR INFORMATION

Corresponding Author

*Phone: +1-650-467-5773. Fax: +1-650-225-2061. E-mail: Fauber.Benjamin@gene.com.

Notes

The authors declare no competing financial interest.

■ ACKNOWLEDGMENTS

We thank Drs. Krista Bowman and Jiansheng Wu, and their respective Genentech research groups, for performing all required protein expression and purification activities. We gratefully acknowledge Yanzhou Liu for NMR support and Antonio G. DiPasquale for solving the crystal structures of **23** and **27**, along with the support of the US NIH Shared Instrumentation grant S10-RR027172 for the purchase of the diffractometer used in this research.

■ ABBREVIATIONS USED

1-ABT, 1-aminobenzotriazole; ADME, adsorption, distribution, metabolism, and excretion; AR, androgen receptor; AUC, area under the curve; BSA, bovine serum albumin; CAR, constitutive androstane receptor; CD, cluster of differentiation; CL_{hep}, predicted hepatic clearance; CL_p, observed plasma clearance; cLogP, calculated Log *P*; C_{max}, maximum plasma concentration; CTG, CellTiter-Glo; CYP, cytochrome P450; DTT, dithiothreitol; ELISA, enzyme-linked immunosorbent assay; ER, estrogen receptor; *F*%, oral bioavailability; FRET, fluorescence resonance energy transfer; FXR, farnesoid X receptor; GM-CSF, granulocyte-macrophage colony stimulating factor; GR, glucocorticoid receptor; GSH, glutathione; GST, glutathione-*S*-transferase; HLM, human liver microsomes; HRP, horseradish peroxidase; HTRF, homogeneous time-resolved fluorescence; IL, interleukin; ILCs, innate lymphoid cells; IFN, interferon; ip, intraperitoneal; iv, intravenous; IVIVc, in vitro to in vivo correlation; LBD, ligand binding domain; LLE, ligand-lipophilicity efficiency; LXR, liver X receptor; MCT, methylcellulose and Tween; MDCK, Madin−Darby canine kidney; MetID, metabolite identification; MLM, mouse liver microsomes; MR, mineralocorticoid receptor; NADPH, nicotinamide adenine dinucleotide phosphate; NOE, nuclear Overhauser effect; NR, nuclear receptor; NSB, nonspecific binding; P_{app}, apparent permeability; PBMC, peripheral blood mononuclear cell; PBS, phosphate-buffered saline; PD, pharmacodynamics; PGR, progesterone receptor; PK, pharmacokinetics; po, oral administration; PPB, plasma-protein binding; PXR, pregnane X receptor; RA, rheumatoid arthritis; RAR, retinoic acid receptor; RLM, rat liver microsomes; RLU, relative luminescence units; ROR, retinoic acid receptor-related orphan receptor; RPMI, Roswell Park Memorial Institute; RuPhos, 2-dicyclohexylphosphino-2′,6′-diisopropoxybiphenyl; RXR, retinoid X receptor; SEM, standard error of the mean; SFC, supercritical fluid chromatography; SRC, steroid receptor coactivator; $t_{1/2}$, half-life; T_H, T helper cell; TGF, transforming growth factor; TR, thyroid receptor; UDPGA, uridine 5′-diphospho-glucuronosyltransferase; V_d, volume of distribution; VDR, vitamin D receptor

■ REFERENCES

(1) Hirose, T.; Smith, R. J.; Jetten, A. M. RORγ: The Third Member of the ROR/RZR Orphan Receptor Subfamily that is Highly Expressed in Skeletal Muscle. *Biochem. Biophys. Res. Commun.* **1994**, *205*, 1976−1983.

(2) Ivanov, I. I.; McKenzie, B. S.; Zhou, L.; Tadokoro, C. E.; Lepelley, A.; Lafaille, J. J.; Cua, D. J.; Littman, D. R. The Orphan Nuclear Receptor RORγt Directs the Differentiation Program of Proinflammatory IL-17$^+$ T Helper Cells. *Cell* **2006**, *126*, 1121−1133.

(3) Bartlett, H. S.; Million, R. P. Targeting the IL-17−T_H17 Pathway. *Nature Rev. Drug Discovery* **2015**, *14*, 11−12.

(4) Pappu, R.; Ramirez-Carrozzi, V.; Ota, N.; Ouyang, W.; Hu, Y. The IL-17 Family Cytokines in Immunity and Disease. *J. Clin. Immunol.* **2010**, *30*, 185−195.

(5) Langley, R. G.; Elewski, B. E.; Lebwohl, M.; Reich, K.; Griffiths, C. E. M.; Papp, K.; Luig, L.; Nakagawa, H.; Spelman, L.; Sigrgeirsson, B.; Rivas, E.; Tsai, F.-F.; Wasel, N.; Tyring, S.; Salko, T.; Hamele, I.; Notter, M.; Karpov, A.; Helou, S.; Papavassilis, C. Secukinumab in Plaque Psoriasis—Results of Two Phase 3 Trials. *N. Engl. J. Med.* **2014**, *371*, 326−338.

(6) Papp, K. A.; Leonardi, C.; Menter, A.; Ortonne, J. P.; Krueger, J. G.; Kricorian, G.; Aras, G.; Li, J.; Russell, C. B.; Thompson, E. H.; Baumgartner, S. Brodalumab, An Anti-Interleukin-17-Receptor Antibody for Psoriasis. *N. Engl. J. Med.* **2012**, *366*, 1181−1189.

(7) Leonardi, C.; Matheson, R.; Zachariae, C.; Cameron, G.; Li, L.; Edson-Heredia, E.; Braun, D.; Banerjee, S. Anti-Interleukin-17 Monoclonal Antibody Ixekizumab in Chronic Plaque Psoriasis. *N. Engl. J. Med.* **2012**, *366*, 1190−1199.

(8) Kellner, H. Targeting Interleukin-17 in Patients with Active Rheumatoid Arthritis: Rationale and Clinical Potential. *Ther. Adv. Musculoskeletal Dis.* **2013**, *5*, 141−152.

(9) Baeten, D.; Baraliakos, X.; Braun, J.; Sieper, J.; Emery, P.; van der Heijde, D.; McInnes, I.; van Laar, J. M.; Landewé, R.; Wordsworth, P.; Wollenhaupt, J.; Kellner, H.; Paramarta, J.; Wei, J.; Brachat, A.; Bek, S.; Laurent, D.; Li, Y.; Wang, Y.; Bertolino, A. P.; Gseiger, S.; Wright, A. M.; Hueber, W. Anti-Interleukin-17A Monoclonal Antibody Secukinumab in Treatment of Ankylosing Spondylitis: A Randomized, Double-Blind, Placebo-Controlled Trial. *Lancet* **2013**, *382*, 1705−1713.

(10) Hueber, W.; Patel, D. D.; Dryja, T.; Wright, A. M.; Koroleva, I.; Bruin, G.; Antoni, C.; Draelos, Z.; Gold, M. H.; Durez, P.; Tak, P. P.; Gomez-Reino, J. J.; Foster, C. S.; Kim, R. Y.; Samson, C. M.; Falk, N. S.; Chu, D. S.; Callanan, D.; Nguyen, Q. D.; Rose, K.; Haider, A.; Di Padova, F. Effects of AIN457, a Fully Human Antibody to Interleukin-17A, on Psoriasis, Rheumatoid Arthritis, and Uveitis. *Sci. Transl. Med.* **2010**, *2*, 52ra72.

(11) Sabat, R.; Ouyang, W.; Wolk, K. Therapeutic Opportunities of the IL-22−IL-22R1 System. *Nature Rev. Drug Discovery* **2014**, *13*, 21−38.

(12) Codarri, L.; Gyülvészi, G.; Tosevski, V.; Hesske, L.; Fontana, A.; Magnenat, L.; Suter, T.; Becher, B. RORγt Drives Production of the Cytokine GM-CSF in Helper T Cells, Which Is Essential for the Effector Phase of Autoimmune Neuroinflammation. *Nature Immunol.* **2011**, *12*, 560−567.

DOI: 10.1021/acs.jmedchem.5b00597
J. Med. Chem. XXXX, XXX, XXX−XXX

(13) Cording, S.; Medvedovic, J.; Cherrier, M.; Eberl, G. Development and Regulation of RORγt$^+$ Innate Lymphoid Cells. *FEBS Lett.* **2014**, *588*, 4176−4181.
(14) Eberl, G.; Marmon, S.; Sunshine, M.-J.; Rennert, P. D.; Choi, Y.; Littman, D. R. An Essential Function for the Nuclear Receptor RORγt in the Generation of Fetal Lymphoid Tissue Inducer Cells. *Nature Immunol.* **2004**, *5*, 64−73.
(15) Pantelyushin, S.; Haak, S.; Ingold, B.; Kulig, P.; Heppner, F. L.; Navarini, A. A.; Becher, B. RORγt$^+$ Innate Lymphocytes and γδ T Cells Initiate Psoriasiform Plaque Formation in Mice. *J. Clin. Invest.* **2012**, *122*, 2252−2256.
(16) Williams, S. C. P. Flurry of Deal-Making Surrounds New Autoimmunity Target. *Nature Med.* **2013**, *19*, 1078.
(17) Yang, J.; Sundrud, M. S.; Skepner, J.; Yamagata, T. Targeting Th17 Cells in Autoimmune Diseases. *Trends Pharmacol. Sci.* **2014**, *35*, 493−500.
(18) Isono, F.; Fujita-Sato, S.; Ito, S. Inhibiting RORγt/Th17 Axis for Autoimmune Disorders. *Drug Discovery Today* **2014**, *19*, 1205−1211.
(19) Fauber, B. P.; Magnuson, S. Modulators of the Nuclear Receptor Retinoic Acid Receptor-Related Orphan Receptor-γ (RORγ or RORc). *J. Med. Chem.* **2014**, *57*, 5871−5892.
(20) Kojetin, D. J.; Burris, T. P. REV-ERB and ROR Nuclear Receptors as Drug Targets. *Nature Rev. Drug Discovery* **2014**, *13*, 197−216.
(21) Kamenecka, T. M.; Lyda, B.; Chang, M. R.; Griffin, P. R. Synthetic Modulators of the Retinoic Acid Receptor-Related Orphan Receptors. *Med. Chem. Commun.* **2013**, *4*, 764−776.
(22) Dhar, M. T. G.; Zhao, Q.; Markby, D. W. Targeting the Nuclear Hormone Receptor RORγt for the Treatment of Autoimmune and Inflammatory Disorders. *Annu. Rep. Med. Chem.* **2013**, *48*, 169−182.
(23) René, O.; Fauber, B. P.; Boenig, G.; Burton, B.; Eidenschenk, C.; Everett, C.; Gobbi, A.; Hymowitz, S. G.; Johnson, A. R.; Kiefer, J. R.; Liimatta, M.; Lockey, P.; Norman, M.; Ouyang, W.; Wallweber, H. A.; Wong, H. Minor Structural Change to Tertiary Sulfonamide RORc Ligands Led to Opposite Mechanisms of Action. *ACS Med. Chem. Lett.* **2015**, *6*, 276−281.
(24) van Niel, M. B.; Fauber, B. P.; Cartwright, M.; Gaines, S.; Killen, J. C.; René, O.; Ward, S. I.; Boenig, G.; Deng, Y.; Eidenschenk, C.; Everett, C.; Gancia, E.; Ganguli, A.; Gobbi, A.; Hawkins, J.; Johnson, A. R.; Kiefer, J. R.; La, H.; Lockey, P.; Norman, M.; Ouyang, W.; Qin, A.; Wakes, N.; Waszkowycz, B.; Wong, H. A Reversed Sulfonamide Series of Selective RORc Inverse Agonists. *Bioorg. Med. Chem. Lett.* **2014**, *24*, 5769−5776.
(25) Fauber, B. P.; René, O.; Boenig, G.; Burton, B.; Deng, Y.; Eidenschenk, C.; Everett, C.; Gobbi, A.; Hymowitz, S. G.; Johnson, A. R.; La, H.; Liimatta, M.; Lockey, P.; Norman, M.; Ouyang, W.; Wang, W.; Wong, H. Reduction in Lipophilicity Improved the Solubility, Plasma-Protein Binding, and Permeability of Tertiary Sulfonamide RORc Inverse Agonists. *Bioorg. Med. Chem. Lett.* **2014**, *24*, 3891−3897.
(26) Fauber, B. P.; René, O.; Burton, B.; Everett, C.; Gobbi, A.; Hawkins, J.; Johnson, A. R.; Liimatta, M.; Lockey, P.; Norman, M.; Wong, H. Identification of Tertiary Sulfonamides as RORc Inverse Agonists. *Bioorg. Med. Chem. Lett.* **2014**, *24*, 2182−2187.
(27) Jiang, L.; Buchwald, S. Palladium-Catalyzed Aromatic Carbon-Nitrogen Bond Formation. In *Metal-Catalyzed Cross-Coupling Reactions*, 2nd ed.; de Meijere, A., Diederich, F., Eds.; Wiley-VCH: Weinheim, 2004; Vol. 2, pp 699−760.
(28) Marco, J. L.; Ingate, S. From α,α-Disubstituted α-Aminonitriles to Heterocycles: Synthesis of Derivatives of 4-Amino-2,3-dihydroisothiazole 1,1-Dioxide, a New Heterocyclic Ring System. *Tetrahedron Lett.* **1997**, *38*, 4835−4836.
(29) Ditrich, K.; Bartsch, M.; Winsel, H. Separation of an Enantiomer Mixture of (*R*)- and (*S*)-3-amino-1-butanol. U.S. Patent 2011/0275855, Nov 10, 2011.
(30) Lee, J.; Zhong, Y.-L.; Reamer, R. A.; Askin, D. Practical Synthesis of Sultams via Sulfonamide Dianion Alkylation: Application to the Synthesis of Chiral Sultams. *Org. Lett.* **2003**, *5*, 4175−4177.
(31) The stereochemistry of the 6-phenyl group for each diastereomer (**24**−**27**) was assigned using NMR and the Karplus relationship, in addition to NOE correlations. The schemes and spectra describing these analyses are shown in the Supporting Information. For additional details, see: (a) Minch, M. J. Orientational Dependence of Vicinal Proton−Proton NMR Coupling Constants: The Karplus Relationship. *Concepts Magn. Reson., Part A* **1994**, *6*, 41−56. (b) Karplus, M. Vicinal Proton Coupling in Nuclear Magnetic Resonance. *J. Am. Chem. Soc.* **1963**, *85*, 2870−2871. (c) Silverstein, R. M.; Webster, F. X.; Kiemle, D. J. *Spectrometric Identification of Organic Compounds*; John Wiley & Sons, Inc.: Hoboken, NJ, 2005; pp 172−175.
(32) (a) March, J. *Advanced Organic Chemistry*, 4th ed.; Wiley-Interscience: New York, 1992; pp 111−112. (b) Eliel, E. L.; Wilen, S. H.; Mander, L. N. *Stereochemistry of Organic Compounds*; John Wiley & Sons, Inc.: New York, 1994; pp 1071−1093.
(33) See the Supporting Information section of the following reference for the detailed biochemical and cellular assay protocols:. Fauber, B. P.; Boenig, G.; Burton, B.; Eidenschenk, C.; Everett, C.; Gobbi, A.; Hymowitz, S. G.; Johnson, A. R.; Liimatta, M.; Lockey, P.; Norman, M.; Ouyang, W.; René, O.; Wong, H. Structure-Based Design of Substituted Hexafluoroisopropanol-arylsulfonamides as Modulators of RORc. *Bioorg. Med. Chem. Lett.* **2013**, *23*, 6604−6609.
(34) Leeson, P. D.; Springthorpe, B. The Influence of Drug-like Concepts on Decision-making in Medicinal Chemistry. *Nature Rev. Drug Discovery* **2007**, *6*, 881−890.
(35) Leach, A. R.; Hann, M. M.; Burrows, J. N.; Griffen, E. J. Fragment Screening: An Introduction. *Mol. BioSyst.* **2006**, *2*, 429−446.
(36) Stepan, A. F.; Karki, K.; McDonald, S.; Dorff, P. H.; Dutra, J. K.; DiRico, K. J.; Won, A.; Subramanyam, C.; Efremov, I. V.; O'Donnell, C. J.; Nolan, C. E.; Becker, S. L.; Pustilnik, R.; Sneed, B.; Sun, H.; Lu, Y.; Robshaw, A. E.; Riddell, D.; O'Sullivan, T. J.; Sibley, E.; Capetta, S.; Atchison, K.; Hallgren, A. J.; Miller, E.; Wood, A.; Obach, R. S. Metabolism-Directed Design of Oxetane-Containing Arylsulfonamide Derivatives as γ-Secretase Inhibitors. *J. Med. Chem.* **2011**, *54*, 7772−7783.
(37) Barnes-Seeman, D.; Jain, M.; Bell, L.; Ferriera, S.; Cohen, S.; Chen, X.-H.; Amin, J.; Snodgrass, B.; Hatsis, P. Metabolically Stable *tert*-Butyl Replacement. *ACS Med. Chem. Lett.* **2013**, *4*, 514−516.
(38) Starting from the X-ray cocrystal structure of the human RORc-LBD and an inverse agonist ligand [PDB: 4WQP], the *N*-isopropyl group was removed from the ligand and two CH_2 groups were added to the remaining *N*-methyl group to close the δ-sultam ring. Minimization of the δ-sultam ring, while keeping all the other ligand and protein atoms fixed, yielded the modeled δ-sultam structure shown in Figure 1. The δ-sultam ring adopted a low-energy chair conformation. The modeling and minimization were done in MOE using the MMFF94x force field (Chemical Computing Group Inc., Montreal, Canada).
(39) Dossetter, A. G.; Griffen, E. J.; Leach, A. G. Matched Molecular Pair Analysis in Drug Discovery. *Drug Discovery Today* **2013**, *18*, 724−731.
(40) In vitro assays to explore the themes of cellular permeability and predicted metabolic clearance have been referred to as in vitro ADME assays. For additional discussion, see Tarbit, M. H.; Berman, J. High-throughput Approaches for Evaluating Absorption, Distribution, Metabolism and Excretion Properties of Lead Compounds. *Curr. Opin. Chem. Biol.* **1998**, *2*, 411−416.
(41) Irvine, J. D.; Takahashi, L.; Lockhart, K.; Cheong, J.; Tolan, J. W.; Selick, H. E.; Grove, J. R. MDCK (Madin−Darby Canine Kidney) Cells: A Tool for Membrane Permeability Screening. *J. Pharm. Sci.* **1999**, *88*, 28−33.
(42) CYP in vitro assay panel included the following isoforms: CYP3A4, CYP2C9, CYP2D6, CYP2C19, and CYP1A2. See the Supporting Information for additional details.
(43) The large NR cell assay panel testing was carried out by Indigo Biosciences (State College, PA) against the following NRs in agonist and antagonist modes using either the full-length NR or a GAL4-NR construct: androgen receptor (AR), constitutive androstane receptor

DOI: 10.1021/acs.jmedchem.5b00597
J. Med. Chem. XXXX, XXX, XXX−XXX

(CAR)-1, CAR2, CAR3, estrogen receptor (ER)-α, ERβ, glucocorticoid receptor (GR), mineralocorticoid receptor (MR), progesterone receptor (PGR), PPARα, PPARβ, PPARγ, retinoic acid receptor (RAR)-α, RARβ, RARγ, retinoid X receptor (RXR)-α, RXRβ, RXRγ, thyroid receptor (TR)-α, TRβ, and vitamin D receptor (VDR). See the Supporting Information for additional details.

(44) The RORb inverse agonist activity of **26** was further supported by the testing of this compound in a RORb SRC1 biochemical assay (EC_{50} = 430 nM, −77% efficacy), analogous to the RORc SRC1 assay described in the manuscript and ref 33.

(45) A team at Phenex Pharmaceuticals recently described a small molecule that was an approximately ten-fold more potent RORc inverse agonist than RORb inverse agonist in cellular assays. Gege, C.; Schlüter, T.; Hoffmann, T. Identification of the First Inverse Agonist of Retinoid-Related Orphan Receptor (ROR) with Dual Selectivity for RORβ and RORγt. *Bioorg. Med. Chem. Lett.* **2014**, *24*, 5265−5267.

(46) Medvedev, A.; Chistokhina, A.; Hirose, T.; Jetten, A. M. Genomic Structure and Chromosomal Mapping of the Nuclear Orphan Receptor RORγ (RORc) Gene. *Genomics* **1997**, *46*, 93−102.

(47) Ortiz, M. A.; Piedrafita, F. J.; Pfahl, M.; Maki, R. TOR: A New Orphan Receptor Expressed in the Thymus that can Modulate Retinoid and Thyroid Hormone Signals. *Mol. Endocrinol.* **1995**, *9*, 1679−1691.

(48) Medvedev, A.; Yan, Y.-H.; Hirose, T.; Giguère, V.; Jetten, A. M. Cloning of cDNA Encoding the Murine Orphan Receptor RZR/RORγ and Characterization of its Response Element. *Gene* **1996**, *181*, 199−206.

(49) Ghoreschi, K.; Laurence, A.; Yang, X. P.; Tato, C. M.; McGeachy, M. J.; Konkel, J. E.; Ramos, H. L.; Wei, L.; Davidson, T. S.; Bouladoux, N.; Grainger, J. R.; Chen, Q.; Kanno, Y.; Watford, W. T.; Sun, H. W.; Eberl, G.; Shevach, E. M.; Belkaid, Y.; Cua, D. J.; Chen, W.; O'Shea, J. J. Generation of Pathogenic T_H17 Cells in the Absence of TGF-β Signaling. *Nature* **2010**, *467*, 971−971.

(50) Takatori, H.; Kanno, Y.; Watford, W. T.; Tato, C. M.; Weiss, G.; Ivanov, I. I.; Littman, D. R.; O'Shea, J. J. Lymphoid Tissue Inducer-like Cells are an Innate Source of IL-17 and IL-22. *J. Exp. Med.* **2009**, *206*, 35−41.

(51) Liu, X.; Wright, M.; Hop, C. E. C. A. Rational Use of Plasma Protein and Tissue Binding Data in Drug Design. *J. Med. Chem.* **2014**, *57*, 8238−8248.

(52) El-Kattan, A. F.; Poe, J.; Buchholz, L.; Thomas, H. V.; Brodfuehrer, J.; Clark, A. The Use of 1-Aminobenzotriazole in Differentiating the Role of CYP-Mediated First Pass Metabolism and Absorption in Limiting Drug Oral Bioavailability: A Case Study. *Drug Metab. Lett.* **2008**, *5*, 120−124.

(53) Under these conditions, IL-17 was primarily produced by γδ T cells and only IL-17FF was detectable in the serum of the mice. For additional discussion, see Sutton, C. E.; Lalor, S. J.; Sweeney, C. M.; Brereton, C. F.; Lavelle, E. C.; Mills, K. H. G. Interleukin-1 and IL-23 Induce Innate IL-17 Production from γδ T cells, Amplifying T_H17 Responses and Autoimmunity. *Immunity* **2009**, *31*, 331−341.

(54) The cytokine stimulation cocktail used in the in vitro murine $CD4^+$ T cell IL-17 production assay (IL-1β, IL-6, and IL-23) closely mimicked the cytokine stimulation cocktail used in the in vivo murine IL-17 PK/PD study (IL-1β and IL-23).

(55) The partition coefficient (Log *P*) was calculated with internal software using the VolSurf approach. For additional details, see Cruciani, G.; Crivori, P.; Carrupt, P.-A.; Testa, B. Molecular Fields in Quantitative Structure−Permeation Relationships: the VolSurf Approach. *THEOCHEM* **2000**, *503*, 17−30.

(56) Condreay, J. P.; Witherspoon, S. M.; Clay, W. C.; Kost, T. A. Transient and Stable Gene Expression in Mammalian Cells Transduced with a Recombinant Baculovirus Vector. *Proc. Natl. Acad. Sci. U. S. A.* **1999**, *96*, 127−132.

(57) Yssel, H.; De Vries, J. E.; Koken, M.; Van Blitterswijk, W.; Spits, H. Serum-Free Medium for Generation and Propagation of Functional Human Cytotoxic and Helper T Cell Clones. *J. Immunol. Methods* **1984**, *72*, 219−227.

(58) Yssel, H.; Spits, H. *Current Protocols in Immunology*; Wiley: New York, 2005; suppl. 65, pp 7.19.1−7.19.12.

DOI: 10.1021/acs.jmedchem.5b00597
J. Med. Chem. XXXX, XXX, XXX−XXX